1

Coordination of KIF3A and KIF13A regulates leading edge localization of MT1-MMP to

promote cancer cell invasion

4

Valentina Gifford, Anna Woskowicz, Noriko Ito, Stefan Balint, Michael L. Dustin, and

Yoshifumi Itoh*

Kennedy Institute of Rheumatology, University of Oxford, Oxford, UK

Running title: MT1-MMP vesicle transport by KIFs promotes cancer cell invasion

9

10

*All correspondence should be addressed to:

Yoshifumi Itoh, PhD

Kennedy Institute of Rheumatology

University of Oxford, Oxford, UK

e-mail: yoshi.itoh@kennedy.ox.ac.uk

16

17

18

19

20

21

ABSTRACT

MT1-MMP plays a crucial role in promoting the cellular invasion of cancer cells by degrading the extracellular matrix to create a path for migration. During this process, its localization at the leading edge of migrating cells is critical, and it is achieved by targeted transport of MT1-MMP-containing vesicles along microtubules by kinesin superfamily proteins (KIFs). Here we identified three KIFs involved in MT1-MMP vesicle transport: KIF3A, KIF13A, and KIF9. Knockdown of KIF3A and KIF13A effectively inhibited MT1-MMP-dependent collagen degradation and invasion, while knockdown of KIF9 increased collagen degradation and invasion. Our data suggest that KIF9 competes with KIF3A/KIF13A to bring MT1-MMP vesicles to different locations in the plasma membrane. Live-cell imaging analyses have indicated that KIF3A and KIF13A coordinate to transport the same MT1-MMP-containing vesicles. Taken together, we have identified a unique interplay between three KIFs to regulate leading edge localization of MT1-MMP and MT1-MMP-dependent cancer cell invasion.

INTRODUCTION

39

40   Invasion and metastasis are the life-threatening features of invasive cancer.

41 Epithelial cancer cells achieve this by losing their cell-cell adhesion property, increasing their

42 motility, and gaining extracellular matrix (ECM) degrading activity for invasion. It has been

43 shown that one of the crucial ECM-degrading enzymes allowing cancer cell invasion and

44 metastasis is membrane-type I matrix metalloproteinase, MT1-MMP(Itoh, 2015; Sabeh et al.,

45 2004; Sabeh et al., 2009; Sato et al., 1994; Seiki, 2003). MT1-MMP is a type-I

46 transmembrane proteinase that belongs to the matrix metalloproteinase (MMP) family. MT1-

47 MMP degrades various ECM components on the cell surface, including fibrillar collagen

48 (Holmbeck et al., 2004; Itoh, 2015; Ohuchi et al., 1997). MT1-MMP also activates proMMP-

49 2 and proMMP-13 on the cell surface, expanding proteolytic repertoire(Itoh, 2015). ProMMP-

50 2 activation is considered essential for epithelial cancer cell invasion and growth since

51 activated MMP-2, but not MT1-MMP, can degrade type IV collagen, a major component of

52 the basement membrane(Itoh, 2015; Taniwaki et al., 2007). MT1-MMP also cleaves

53 membrane proteins, including CD44(Kajita et al., 2001), ICAM-1(Sithu et al., 2007),

54 LRP1(Rozanov et al., 2004), syndecan 1(Endo et al., 2003), ADAM9(Chan et al., 2012),

55 Dll1(Jin et al., 2011), EphA2(Koshikawa et al., 2015; Sugiyama et al., 2013), modifying cell

56 adhesion property and cellular signalling. Thus, MT1-MMP is considered to be a

57 microenvironment and cell function modifier.

58   Localization of MT1-MMP at the leading edge of migrating cells is crucial to promote

59 cellular invasion(Ferrari et al., 2019; Gifford and Itoh, 2019; Itoh, 2015). Leading-edge

60 structures or their precursors include filopodia, lamellipodia, invadopodia, and podosomes,

61 and MT1-MMP localizes to all of these structure(Ferrari et al., 2019; Gifford and Itoh, 2019;

62 Itoh, 2015). MT1-MMP also localizes at focal adhesion (FA)(Wang and McNiven, 2012;

63 Woskowicz et al., 2013). It is thought that localization of MT1-MMP is achieved by direct

64 transport of MT1-MMP-containing vesicles to these membrane structures(Wiesner et al.,

65 2010), but the mechanism of vesicle transport of MT1-MMP is still poorly understood.

66 Vesicle transport is carried out by motor proteins, including kinesin superfamily proteins

3

67   (KIFs), which transport vesicles and macromolecules along microtubules(Hirokawa et al.,

68   2009; Hirokawa and Tanaka, 2015). There are 45 KIFs in humans that are classified into

69   three groups, N-, M- and C-kinesins, according to the position of the microtubule-binding

70   motor domain(Hirokawa and Tanaka, 2015). KIFs that transport vesicles toward the cell

71   periphery or the (+) ends of microtubules belong to N-kinesins, which form the largest

72   subgroup of 39 KIFs and can be further divided into 11 subgroups(Hirokawa et al., 2009;

73   Hirokawa and Tanaka, 2015). N-kinesins have a motor domain at their N-terminus, followed

74   by a neck region, a coiled-coil region, and a C-terminal tail region(Hirokawa et al., 2009;

75   Hirokawa and Tanaka, 2015). It is thought that each KIF can selectively recognize certain

76   cargos through the specific interaction with adaptor molecules, membrane proteins, or Rab

77   GTPases through their C-terminal tail region. So far, KIF5B and KIF3A/B have been

78   reported to transport MT1-MMP vesicles in macrophages (Wiesner et al., 2010). KIF5B and

79   KIF3A have been reported to play a role in invadopodia localization of MT1-MMP in MDA-

80   MB231 cells (Marchesin et al., 2015; Thapa and Anderson, 2017). However, the roles of

81   KIFs in MT1-MMP vesicles trafficking in different cells are not understood.

82   This study aimed to identify KIFs responsible for MT1-MMP localization at the

83   leading edge of invasive human fibrosarcoma, HT-1080. By screening with siRNAs, we

84   identified three KIFs (KIF3A, KIF13A, and KIF9) directly involved in MT1-MMP vesicle

85   trafficking. We report here the co-ordination of KIF3A and KIF13A to transport MT1-MMP

86   vesicles and the potential competitive role of KIF9 against KIF3A and KIF13A.

87

88   **RESULTS**

89   **Knockdown of KIF13A, KIF3A, KIF9 and KIF1C alters MT1-MMP-medited cell functions**

90   **on the cell surface**

91   To identify KIFs responsible for MT1-MMP vesicle transport, we initially narrowed

92   down the candidate KIFs. There are 45 KIFs in humans, and we initially excluded C- and M-

93   kinesins since they do not traffic to the (+) ends of microtubules. We further excluded KIFs

94   reported to be exclusively expressed in neurons or involved in cell division as they are

95   unlikely to control MT1-MMP vesicle trafficking (Supplementary Table S1). This exercise

96   leaves 17 KIFs, including splicing variants, as candidates for screening. In order to screen

97   KIFs necessary for MT1-MMP trafficking, we set up a gelatin and collagen film degradation

98   assay with HT-1080 cells. As shown in Supplementary Figure S1a-d, gelatin and collagen

99   film degradation were abolished by a broad-spectrum MMP inhibitor GM6001 (10 μM) and

100   by a specific biologic MT1-MMP inhibitor DX-2400 (200nM)(Devy et al., 2009), but not by

101   TIMP-1 (200 nM), which does not inhibit MT1-MMP but inhibits all soluble and GPI-anchored

102   MMPs. The data suggested that both gelatin and collagen film degradation activities are

103   solely dependent on endogenous MT1-MMP in HT1080 cells. We confirmed that HT-1080

104   cells expressed all 17 KIFs (Supplementary Fig S2a), each KIF gene was silenced by siRNA,

105   and cells were subjected to gelatin film degradation assay (Figure S2b, c). Among the 17

106   KIFs, knockdown of KIF1C, KIF3A, and KIF13A notably decreased gelatin film degradation,

107   while knockdown of KIF9 rather increased gelatin film degradation (Figure S2b). Therefore,

108   we investigated KIF1C, 3A, 13A and 9 further.

109   Knockdown of KIF13A, KIF3A, and KIF1C notably decreased MT1-MMP-mediated

110   gelatin film degradation, whereas the knockdown of KIF9 enhanced it in a statistically

111   significant manner compared to non-targeting siRNA (si-NT) transfected cells (P < 0.0001)

112   (Figure 1a). Western Blotting for KIF3A and KIF1C and by RT-PCR for KIF13A and KIF9

113   (Figure 1d, top and middle panels) confirmed the efficiency of silencing. Interestingly, siRNA

114   for KIF9 by smart pool siRNA (si-KIF9) was selective for KIF9-v1 (knocked down by more

115   than 90%), as KIF9-v2 and -3 mRNA level were knocked down only by 39%. We also

116   confirmed that silencing any of these *kinesin* genes did not alter MT1-MMP mRNA levels

117   (Figure 1d, bottom panel). Since it has been reported that KIF5B mediates MT1-MMP

118   intracellular trafficking in primary macrophages and breast cancer cell line, MDA-

119   MB231(Marchesin et al., 2015; Thapa and Anderson, 2017; Wiesner et al., 2010), we also

120   re-examined KIF5B knockdown in HT-1080 cells. We confirmed that KIF5B knockdown did

121   not affect gelatin film degradation (Figure 1e). Next, we examined the effect of KIF

122   knockdown on the collagenolytic activity of MT1-MMP in HT-1080 cells as the type I collagen

123   represents its physiological substrate. As shown in Figure 1b, KIF13A, KIF3A, and KIF1C

124   knockdowns decreased collagen degradation by HT1080 cells, while the knockdown of KIF9

125   enhanced it in a statistically significant manner (Figure 1b, right panel).

126   Another cell surface activity of MT1-MMP is proMMP-2 activation. ProMMP-2

127   activation can be induced by adding collagen I (100 μg/ml) in the culture medium(Majkowska

128   et al., 2017). We confirmed that the collagen-induced proMMP-2 activation is due to MT1-

129   MMP in HT-1080 cells (Supplementary Figure S1e, f). As indicated in Figure 1c, the

130   conditioned medium from si-NT-transfected cells, without collagen, showed proMMP-2

131   (ProMMP-2, 68 kDa) and its intermediate form (Intermediate, 65 KDa) (Figure 1c, left panel).

132   Silencing *Kif13a*, *Kif3a,* and *Kif1c* genes prevented the generation of the intermediate form,

133   whereas silencing the *Kif9* gene accelerated proMMP-2 processing to its intermediate and

134   active forms (Active form, 62 kDa, Figure 1c, left panel). Upon collagen stimulation, around

135   71% of proMMP-2 was converted to its active form in si-NT-transfected cells (Figure 1c,

136   center lower panel). The knockdown of KIF13A and KIF3A significantly reduced the

137   activation down to 26% and 25%, respectively. Knockdown of KIF1C seemed to moderately

138   decrease it to 44% (Figure 1c, center lower panel). Conversely, silencing the *Kif9* gene

139   enhanced the activation to around 80% in a statistically significant manner (Figure 1c, center

140   lower panel). Interestingly, we noted that the generation of the 45 KDa processed form of

141   MT1-MMP, which has been shown to coincide with functional activation of MT1-MMP, was

142   also affected by KIF knockdown (Figure 1c, left panel)(Stanton et al., 1998). The knockdown

143   of KIF13A, KIF3A, and KIF1C significantly reduced the generation of the 45 kDa form

144   (Figure 1c, left and right panels), while the knockdown of KIF9 have a tendency to increase

145   it. However, the effect was statistically not significant (Figure 1c, left and right panels).

146

147   **Knockdown of KIF13A, KIF3A, KIF9 and KIF1C alters MT1-MMP localization at the cell-**

148   **matrix interface**

149   The cell surface biotinylation experiment indicated that KIF knockdown did not affect

150   the overall cell surface level of MT1-MMP (Figure 2a). This result was also confirmed by

151   immunofluorescence staining of the cell surface MT1-MMP (Figure 2b). Therefore, we

152   hypothesized that the KIF knockdown shifts the localization of MT1-MMP to or from the cell-

153   matrix interface. We employed total internal reflection fluorescent (TIRF) microscopy to

154   examine the levels of MT1-MMP at the ventral side of the membrane. As shown in Figure

155   2c, silencing *Kif13a* and *Kif3a* genes significantly reduced MT1-MMP localization at the cell-

156   matrix interface, whereas the knockdown of KIF9 increased it (Figure 2c). Knockdown of

157   KIF1C did not change MT1-MMP localization significantly (Figure 2c). The knockdown of

158   these KIFs did not influence cellular attachment to the gelatin, as it did not impact the level

159   of β1 integrin (Figure 2d) and close cell-matrix contacts detected by interference reflection

160   microscopy (IRM) (Figure 2d, top panel). Taken together, these data indicate that knocking

161   down KIF3a, KIF13a and KIF9 altered MT1-MMP-dependent activity by changing the level of

162   MT1-MMP localization at the cell-matrix interface.

163

164   **The knockdown of KIF13A, KIF3A and KIF9 alters MT1-MMP-mediated cell invasion**

165   **through a microporous membrane and MT1-MMP-dependent cell migration in 3D**

166   **collagen.**

167   We next examined the effect of KIF knockdown on MT1-MMP-dependent cell

168   invasion. We employed two different invasion assays: collagen invasion assay using trans-

169   well chambers coated with collagen gel (Figure 3a) and microcarrier bead invasion assay

170   that assesses migration distance of cells from the beads' surface within 3D collagen gel

171   (Figure 3b). The cellular invasion in these assays is entirely dependent on endogenous

172   MT1-MMP in HT-1080 cells (Figure S1f, g). As shown in Figure 3a (bottom right panel), the

173   knockdown of KIF13A and KIF3A significantly decreased the invasion, whereas KIF9

174   knockdown significantly enhanced it in the trans-well invasion assay. KIF1C knockdown did

175   not affect the cell invasion (Figure 3a, bottom right panel). In microcarrier bead invasion

176   assay (Figure 3b), the knockdowns of KIF13A, KIF3A, and KIF1C significantly reduced cell

177   migration. Interestingly, si-KIF9-transfected cells also migrated significantly less (Figure 3b),

178   which is contrary to the trans-well invasion assay (Figure 3a). The effect of knockdown of

7

179   KIF13A, KIF3A, and KIF9 on cellular invasion was not due to alteration on the fundamental

180   cell migration machinery. These cells migrated similarly on the plastic surface as measured

181   by a wound-healing assay (Figure 3c). On the other hand, KIF1C knockdown slightly

182   decreased it (P = 0.019), indicating that KIF1C may be involved in the general cell migration

183   (Figure 3c).

184

185   **KIF13A and KIF3A co-localize with MT1-MMP-containing vesicles**

186   Next, the cellular distribution of MT1-RFP and GFP-tagged KIF13A, KIF3A, KIF9-v1,

187   KIF9-v2, and KIF1C were analyzed. As shown in Figure 4a, KIF13A-GFP co-localized with

188   MT1-RFP, and the two proteins exhibited a similar distribution pattern within the perinuclear

189   (white box) and the cell periphery areas (orange box). KIF3A-GFP also co-localized with

190   MT1-RFP-positive vesicles within the perinuclear region (Figure 4b, white box), but the two

191   proteins did not colocalize at the cell periphery (Figure 4b, orange box). KIF9-v1-GFP

192   colocalized with MT1-RFP within the perinuclear region (Figure 4c, White box), but not cell

193   periphery (Figure 4c, orange box). KIF9-v2-GFP- and KIF1C-GFP-transfected cells did not

194   show a clear vesicular-like distribution of MT1-RFP clearly, and neither KIF9-v2-GFP nor

195   KIF1C-GFP showed co-localization with MT1-RFP neither in perinuclear nor cell periphery

196   region (Figure 4d and e). It was interesting to note that KIF1C-GFP strongly accumulated at

197   the tips of the trailing edges (Figure 4e, orange box). Pearson's correlation coefficients

198   (PCCs) confirmed that KIF13A-GFP and KIF3A-GFP had the highest degree of co-

199   localization (Figure 4f). On the other hand, KIF9-v2-GFP and KIF1C-GFP exhibited the least

200   co-localization with MT1-RFP. These cells were also embedded in a 3D collagen matrix and

201   imaged by confocal microscopy (Figure 4g-i). The data confirmed that KIF13A-GFP

202   exhibited the highest co-localization with MT1-RFP (Figure 4g, i), whereas KIF3A-GFP co-

203   localization was found only within the perinuclear region (Figure 4h, i). We confirmed no co-

204   localization of KIF9-v2-GFP and KIF1C-GFP with MT1-RFP under these conditions (Figure

205   4j-i).

206

207   KIF13A, KIF3A and KIF9-v1 transport MT1-MMP-containing vesicles

208   These cells were next subjected to time-lapse imaging using confocal microscopy.

209   The expression of KIF13A-GFP often made a distribution of MT1-RFP signals into a tubular-

210   like shape, extending from the perinuclear regions towards the tips of the ruffling membrane

211   (Figure 5a). Numerous KIF13A-GFP signals were observed moving along these MT1-RFP

212   tubular-like structures, accumulating at the cell periphery, suggesting that the tubular-like

213   structures are microtubules, and MT1-RFP seems to be distributed over the microtubules

214   (supplemental *movie S1*). Vesicles double positive for KIF13A-GFP and MT1-RFP could

215   also be detected within the perinuclear area. Despite MT1-RFP strongly accumulated within

216   this region, it was possible to observe KIF13A-GFP transporting MT1-RFP-containing

217   vesicles (Figure 5b, *movie S2).* No significant differences were observed in velocity or size

218   of vesicles between the the cell periphery or within the perinuclear area (Figure 5c, d).

219   We also carried out live cell imaging on TIRF microscopy (Figure 5e, *movie S3*) and

220   the vesicles positive for KIF13A-GFP and MT1-RFP were detected at the cell-matrix

221   interface. Combining time-lapse IRM with time-lapse TIRF microscopy, we also observed

222   that MT1-RFP progressively accumulated at the growing adherent membrane on a gelatin-

223   coated glass surface (Figure 5f). As discussed above, MT1-RFP-positive vesicles were

224   again distributed in tubular-like structures, which pointed toward the growing highly adherent

225   membrane (Figure 5f, *movie S4)*

226   Expression of KIF3A-GFP in HT-1080 cells did not affect the shape of MT1-RFP-

227   positive vesicles (Figure 5g, h). The vesicles positive for KIF3A-GFP and MT1-RFP were

228   either moving linearly (Figure 5g, *movie S5*) or oscillatory within the perinuclear region

229   (Figure 5h, *movie S6*). Their mean velocities and diameters were equal, regardless of their

230   trajectory (Figure 5i, j).

231   Vesicles double positive for KIF9-v1-GFP and MT1-RFP were detected within the

232   perinuclear area of HT-1080 cells (Figure 6a). These vesicles did not move, but their

233   fluorescence intensity faded over time, suggesting that the vesicles moved out of the focus

234   plane, along the z-axis, most likely towards the dorsal side of the cell. As shown in

9

235   Supplementary Figure 6b, no vesicles positive for both KIF9-v2-GFP and MT1-RFP could be

236   detected. Likewise, we could not observe any MT1-RFP-positive vesicles trafficked by

237   KIF1C-GFP (Figure 6c). Once more, KIF1C-GFP was accumulated at the trailing edge

238   (Figure 6c).

239

240   **Collaboration of KIF13A and KIF3A and competition of KIF9-v1 with KIF13A/KIF3A to**

241   **transport MT1-MMP vesicles**

242   We next investigated if KIF13A and KIF3A transport MT1-MMP vesicles

243   independently or in collaboration. HT-1080 cells transfected for si-KIF13A, si-KIF3A, and a

244   combination of the two were subjected to gelatin film degradation (Figure 7a, b, c). If these

245   KIFs work independently, double knockdown of KIF3A and KIF13A should show additive

246   inhibitory effect. However, if they work in collaboration, such an effect should not be

247   observed. Upon KIF13A knockdown, gelatin film degradation was decreased by around

248   78%, while KIF3A knockdown by 49%. When the two knockdowns were combined, gelatin

249   film degradation was decreased by 82%, which is the same level as KIF13A knockdown

250   alone (Figure 7a, b). These data suggest that these two motor proteins function on the same

251   pathway to deliver MT1-MMP to the cell surface.

252   Next, HT-1080 cells expressing KIF13A-GFP, KIF3A-HaloTag, and MT1-RFP were

253   subjected to time-lapse imaging. Vesicles positive for all three signals were detected within

254   the perinuclear region (Figure 7d, e). As pointed by the arrows colored according to the

255   different channels, these vesicles moved from the perinuclear area towards the cell

256   periphery (Figure 7d). KIF13A-GFP and KIF3A-HaloTag co-localized with MT1-RFP-,

257   containing vesicle until MT1-RFP fluorescence signal had faded, indicating that the MT1-

258   RFP vesicle had fused with the plasma membrane (Figure 7d). Then, KIF13A-GFP and

259   KIF3A-HaloTag independently trafficked back towards the center of the cell (Figure 7d). In

260   other cases, these vesicles positive for KIF13A-GFP, KIF3A-HaloTag, and MT1-RFP were

261   oscillating within the perinuclear region (Figure 7e). On the other hand, vesicles at the cell

262   periphery were positive for only KIF13A-GFP and MT1-RFP (Figure 7f, *movie S7*). These

263   vesicles were either moving within the cell edge or the perinuclear region. Interestingly, with

264   KIF3A-HaloTag expression, KIF13A-GFP- and MT1-RFP-positive vesicles moved

265   significantly faster at the cell edge within the perinuclear area (Figure 7g). With KIF13A-GFP

266   expression, KIF3A-HaloTag- and MT1-RFP-positive vesicles moved significantly faster when

267   they were proceeding with a linear trajectory than when they were oscillating (Figure 7h).

268   Taken together, we concluded that KIF13A and KIF3A co-traffic MT1-MMP-containing

269   vesicles around the perinuclear areas, and KIF13A takes over the vesicles at the periphery

270   to traffic them towards the plasma membrane of the cell.

271   Given the role of KIF3A and KIF13A in MT1-MMP vesicle transport to degrade

272   matrix, increased matrix-degrading activity upon KIF9 knockdown may be due to increased

273   KIF3A and KIF13A-mediated vesicle transport of MT1-MMP. To test this hypothesis, *Kif9*

274   was co-silenced with *Kif3a* or *Kif1a.* As shown in Figure 8, increased gelatin film

275   degradation by KIF9 knockdown was significantly decreased upon co-silencing *Kif3a or*

276   *Kif13a* genes. These data suggest that knockdown of KIF9 made MT1-MMP vesicles

277   available for KIF3A- and KIF13A-dependent vesicle transport, resulting in increased matrix

278   degradation.

279

280   **Role of KIF13A, KIF3A, KIF9 and KIF1C in MT1-MMP secretion in other cell types**

281   We next investigated the role of these KIFs in other cell types. First, human

282   rheumatoid arthritis synovial fibroblasts (RASFs) were examined since RASFs' cell surface

283   collagenolytic activity is solely MT1-MMP-dependent (Kaneko et al., 2016; Majkowska et al.,

284   2017; Miller et al., 2009). RASFs from three different donors were transfected with siRNAs

285   targeting these four KIFs and subjected to collagen film degradation assay. As shown in

286   Figure 9 (a-c), knockdown of KIF13A and KIF3A significantly reduced collagen film

287   degrading activity, while KIF9 knockdown enhanced it. KIF1C knockdown did not influence

288   the collagen degradation. These data suggest that KIF13A, KIF3A, and KIF9 are similarly

289   involved in MT1-MMP intracellular trafficking in RASFs.

290   Next, triple-negative breast cancer cell line, MDA-MB-231 cells were examined.

291   MDA-MB-231 cells have been characterized extensively for invadopodia-mediated cell

292   invasion, which is also MT1-MMP-dependent (Castro-Castro et al., 2016; Ferrari et al., 2019;

293   Frittoli et al., 2011; Infante et al., 2018; Poincloux et al., 2009). MDA-MB-231 cells were

294   transfected with siRNAs targeting KIF13A, KIF3A, KIF9, KIF1C, and KIF5B and subjected to

295   gelatin film degradation (Figure 9d-f). Interestingly, silencing these five *kinesin* genes,

296   including KIF3A and KIF5B previously shown to associate with MT1-MMP-containing

297   vesicles in MDA-MB-231 cells (Marchesin et al., 2015; Wang et al., 2017), did not impact

298   MT1-MMP- and invadopodia-dependent gelatin film degradation (Figure 9d, e). These data

299   suggest that roles of KIFs in trafficking MT1-MMP-containing vesicles are cell context-

300   dependent.

301

302   **Genomic alterations of *Kif13a* and *Kif9* genes across The Cancer Genome Atlas**

303   **(TCGA) studies**

304   We next investigated if expression level of KIF3A, KIF13A and KIF9 have any

305   correlation with cancer progression. Gene expression of KIF13A, KIF3A, and KIF9 across

306   The Cancer Genome Atlas (TCGA) PanCancer Atlas studies were analyzed. Amplifications

307   and deep deletions of *Kif13a*, *Kif3a,* and *Kif9* genes across the TCGA database were

308   searched on cBioPortal (http://cbioportal.org)(Cerami et al., 2012; Gao et al., 2013). The

309   term amplification indicates a high copy-number level per gene. Deep deletion implies a

310   profound loss in the copy-number level per gene and often refers to a homozygous deletion.

311   As shown in Figure 10a, the *Kif13a* gene was amplified in 1.3% of samples across the

312   TCGA PanCancer Atlas studies and deleted in 0.2%. On the other hand, the *Kif9* gene was

313   amplified in only 0.1% of samples and deleted in 0.5%. These gene alterations were

314   distributed across several cancer types of TCGA (Figure 10b, c). More than seven in 100

315   women diagnosed with ovarian serous cystadenocarcinoma presented a *Kif13a* gene

316   amplification (Figure 10b). *Kif13a* gene was also amplified in more than 6% and 4% of

317   patients diagnosed with bladder urothelial cancer and diffuse large-B cell lymphoma (DLBC),

12

318 respectively (Figure 10b). *Kif9* gene was deleted in over 6 out of 100 patients diagnosed with

319 DLBC and in almost 3% of patients with kidney renal clear cell carcinoma (ccRCC) (Figure

320 9c). Next, we used the Pathology Atlas

321 (https://www.proteinatlas.org/humanproteome/pathology)(Uhlen et al., 2017) to investigate

322 whether KIF13A and KIF9 are considered prognostic markers for specific cancer types. We

323 performed Kaplan-Meier survival analysis of liver cancer patients with low or high mRNA

324 expression of the *Kif13a* gene through the Pathology Atlas. We found that patients with high

325 expression of the *Kif13a* gene had a significantly lower survival rate (Figure 10d). We also

326 performed the same analysis of renal and colorectal cancer patients with low or high mRNA

327 expression of the *Kif9* gene. We found that patients with low expression had a significantly

328 lower survival rate (Figure 10e, f).

329   *Kif3a* gene was amplified in 0.5% of cases across the TCGA PanCancer Atlas

330 studies and deleted in 0.3% of them (Figure S3a). 5% of patients with ccRCC presented an

331 amplification of the *Kif3a* gene. However, we could not assess whether this gene alteration

332 was associated with a change to the overall patients' survival (Figure S3b). According to our

333 search on the Pathology Atlas, *Kif3a* gene alterations are not considered prognostic markers

334 for different cancer types.

335

336 **DISCUSSION**

337   When invading cancer cells encounter a physical ECM barrier with narrow gaps of

338 less than 7 µm in diameter, they utilize MT1-MMP to break through the barrier and create a

339 path for migration (Wolf et al., 2013). In this process, cells directly secrete MT1-MMP to the

340 invading edge by trafficking MT1-MMP-containing vesicles along microtubules. Here, we

341 have identified three kinesin motor proteins, KIF3A, KIF13A, and KIF9, directly involved in

342 the trafficking of MT1-MMP-containing vesicles to the leading edge.

343   Although knockdown of KIF1C significantly reduced gelatin and collagen film

344 degradation like KIF3A and KIF13A knockdown, we could not get the evidence that KIF1C

345 was directly involved in MT1-MMP vesicle transport. MT1-RFP and KIF1C-GFP did not co-

13

346   localize when cells were cultured either on a gelatin film or within 3D collagen gel, and there

347   was a strong tendency of KIF1C to localize at the trailing edge of migrating cells rather than

348   at the leading edge. A similar conclusion was made by Weisner *et al.*(Wiesner et al., 2010),

349   as they observed that KIF1C knockdown decreased MT1-MMP-dependent gelatin film

350   degradation at podosomes, but KIF1C did not co-localize with MT1-MMP vesicles. KIF1C

351   may affect MT1-MMP vesicle transport indirectly, by potentially influencing cell migration

352   machinery, as knockdown of KIF1C, but not other KIFs, reduced cell migration on plastic

353   significantly (Figure 3c), which is an MT1-MMP-independent process. Therefore, KIF3A and

354   KIF13A are the major KIFs that directly traffic MT1-MMP vesicles to the leading edge in

355   HT1080 cells.

356   Interestingly, the same effect of knockdown of KIF3A, KIF13A and KIF9 was also

357   observed for proMMP-2 activation activity. We and others have previously reported that

358   homodimer formation of MT1-MMP is essential for proMMP-2 activation on the cell surface

359   to form a proMMP-2 activation complex of $(MT1\text{-}MMP)_2$-TIMP-2-proMMP-2 (Gifford and Itoh,

360   2019; Itoh, 2015; Itoh et al., 2001; Lehti et al., 2002). We have previously reported that

361   homodimerization of MT1-MMP occurs consistently at the leading edge of invading cells

362   regulated through the re-organization of the cytoskeletal actin by Rac1 and Cdc42 (Itoh et al.,

363   2011). Thus, the leading-edge localization of MT1-MMP via the vesicle transport by KIF3A

364   and KIF13A may closely associate with proMMP-2 activation activity.

365   Our data suggest that MT1-MMP vesicles were initially trafficked by both KIF3A and

366   KIF13A in coordination around the perinuclear area, and then KIF13A alone further

367   transports the vesicles to the leading edge. To our knowledge, this is the first example of

368   coordinated vesicle transport between KIF3A and KIF13A. KIF3A belongs to the kinesin-2

369   subfamily and has been shown to play a crucial role in the primary cilium formation

370   (Hirokawa, 2000). It was shown that KIF3 is involved in post-Golgi transport of N-cadherin/*β*-

371   catenin, which plays a role in the adhesion of neuronal progenitor cells (Teng et al., 2005).

372   KIF13A belongs to the kinesin-3 subfamily and is known to mediate vesicle transport from

373   the endosomal recycling compartment to the plasma membrane (Hirokawa et al., 2009;

374   Nakagawa et al., 2000; Perez Bay et al., 2013). It has been shown that KIF13A, together

375   with Rab22A and BLOCK1/2, plays a central role in the biogenesis of recycling endosomes

376   (Shakya et al., 2018). Trans-Golgi network (TGN) is the last station of the secretory pathway

377   of proteins, and after TGN, the cargo can be trafficked to three destinations: 1) the plasma

378   membrane, 2) the secretory granules, and 3) the endosomes (Le Borgne and Hoflack, 1998).

379   MT1-MMP is stored in endosomes upon endocytosis (Jiang et al., 2001; Planchon et al.,

380   2018; Remacle et al., 2003), and during exocytosis (Pedersen et al., 2020). With our data

381   that KIF13A knockdown significantly inhibited MT1-MMP activity on the cell surface, we

382   speculate that KIF3A and KIF13A transport MT1-MMP vesicles from TGN to the endosome,

383   and KIF13A further transports the vesicles from the endosomes to the plasma membrane.

384   There are three splicing variants of KIF9, KIF9-v1, -v2, and -v3. KIF9-v2 and -v3

385   encode identical amino acid sequences, while KIF9-v1 is 65 amino acids shorter in the

386   coiled-coil region. Upon KIF9 knockdown using smart pool siRNA, KIF9-v1 was selectively

387   knocked down. Interestingly co-localization with MT1-MMP vesicles was only observed with

388   KIF9-v1, but not KIF9-v2. Therefore, increased gelatin and collagen film degradation and

389   proMMP-2 activation resulted from KIF9 knockdown were most likely attributed to KIF9-v1

390   knockdown, which is the first example of functional difference between KIF9 variants.

391   However, it is not clear why KIF9-v1, but not KIF9-v2, is selectively involved in MT1-MMP

392   vesicle transport since KIF9-v1 and v2 share the same C-terminal tail region, where these

393   KIFs are thought to interact with the cargo. Further investigation is required.

394   Live-cell imaging data indicated that the vesicles positive for MT1-RFP and KIF9-v1-

395   GFP did not move much in a lateral direction. However, they faded out from the focus plane

396   over time, suggesting that KIF9 may carry the vesicles to the dorsal side of the cell surface.

397   Increased gelatin film degradation upon KIF9 knockdown was inhibited by co-silencing

398   *kif13a* or *kif3a* genes, suggesting that the increased degradation is due to increased

399   KIF13A- and KIF3A-dependent MT1-MMP vesicle transport to the matrix attachment sites. It

400   is thus possible that KIF9-v1 competes with KIF13A and KIF3A to bring MT1-MMP-

401   containing vesicles to different plasma membrane domains. Upon KIF9-v1 knockdown,

402   vesicle transport by KIF13A and KIF3A starts to dominate, resulting in increased matrix

403   degradation.

404   KIF9 knockdown increased cellular invasion in trans-well invasion assay, with the

405   same tendency observed for gelatin and collagen film degradations. However, KIF9

406   knockdown significantly reduced cell migration in microcarrier beads invasion assay. This

407   seemingly contradictory result can be due to differences between the two invasion assay

408   systems. The first difference is whether cells face the collagen only at the ventral side (trans-

409   well system) or surrounded by collagen fibrils (micro-carrier beads system). Another

410   difference can be whether the migration is chemoattractant-guided or matrix-guided. In the

411   trans-well system, the lower chamber contained 10% FBS, while the upper chamber was

412   serum-free. Thus, cells in the upper chamber are attracted by the serum components such

413   as lysophosphatidic acid (Idzko et al., 2004) in the lower chamber. In the microcarrier beads

414   invasion assay, there are no chemoattractant gradients. Thus, cells are instead guided by

415   collagen fibrils. When cells migrate through the 3D collagen matrix, cells enlarge the gaps of

416   collagen fibrils by degrading it at the middle of pseudopods in a ring shape (Wolf et al., 2013;

417   Wolf et al., 2007). KIF9 may be involved in the vesicle trafficking of MT1-MMP to these

418   regions of the plasma membrane in coordination with KIF3A and KIF13A. KIF9 was

419   previously shown to be involved in gelatin degradation at podosomes in macrophages

420   (Cornfine et al., 2011). In that report, they found that reggie/flotillin interacts with the C-

421   terminal cargo binding domain of KIF9, and knockdown of KIF9 or flotillin significantly

422   reduced gelatin degradation at the podosomes (Cornfine et al., 2011). However, it was

423   concluded that KIF9 was not directly involved in MT1-MMP vesicle transport to the

424   podosomes in macrophages (Cornfine et al., 2011; Wiesner et al., 2010).

425   Our data in this study indicate that knockdown of KIF3A and KIF13A in human

426   RASFs significantly reduced collagen film degradation. In contrast, KIF9 knockdown

427   enhanced it (Figure 8), suggesting that RASFs share the same vesicle transport mechanism

428   with HT1080 cells. On the other hand, knockdown of KIF3A, KIF13A, KIF9 did not influence

429   invadopodia-mediated gelatin film degradation in MDA-MB231 cells (Figure 9d, e). Thus,

16

430   motor proteins responsible for MT1-MMP vesicle transport are cell context-dependent. It has

431   been reported that KIF5B and KIF3A/KIF3B are the responsible KIFs in trafficking MT1-MMP

432   vesicles to the podosome in macrophages (Wiesner et al., 2010). KIF5B and KIF3A were

433   also shown to mediate MT1-MMP vesicle transport to the invadopodia in MDA-

434   MB231(Marchesin et al., 2015). However, our data indicate that knockdown of none of the

435   KIFs we examined, including KIF5B, KIF13A, KIF3A, KIF9, and KIF1C, influenced

436   invadopodia-mediated gelatin film degradation in MDA-MB231 cells. In HT1080 cells, KIF5B

437   knockdown did not influence gelatin film degradation as well. One of the differences between

438   these reports and our data is that we have analyzed endogenous MT1-MMP activity on the

439   cell surface in both MDA-MB231 and HT1080 cells, while in these reports, KIF5B

440   involvement was investigated on ectopically expressed mCherry-tagged MT1-MMP in both

441   macrophages and MDA-MB231 (Marchesin et al., 2015; Wiesner et al., 2010). Since

442   mCherry was inserted at the C-terminus of the cytoplasmic domain of MT1-MMP (Marchesin

443   et al., 2015; Wiesner et al., 2010), the vesicle transport pathway of MT1-mCherry may differ

444   from endogenous wild-type MT1-MMP. It is also possible that overexpressed enzyme may

445   gain alternative vesicle trafficking pathways. Another possibility might be related to different

446   cell types and culture conditions. Macrophages may potentially have a different mechanism

447   of MT1-MMP vesicle trafficking from HT1080 cells, and MDA-MB231 cells in different lab

448   may gain different mechanism. Nevertheless, we have concluded that KIF5B is not involved

449   in vesicle transport of endogenous MT1-MMP in HT1080 cells.

450   The analysis of the TCGA database revealed that the expression profile of KIF13A

451   and KIF9 is altered in several cancer types. Amplification is the most common *Kif13a* gene

452   alteration detected across the TCGA database. KIF13A is reported by the Pathology Atlas

453   (https://www.proteinatlas.org/humanproteome/pathology) (Uhlen et al., 2017) as an

454   unfavorable prognostic marker for liver cancer patients. As shown in Figure 10, liver cancer

455   patients with a high expression of KIF13A had a significantly lower survival probability than

456   those with a low expression. Our data suggest that KIF13A is a crucial player of MT1-MMP

457   intracellular trafficking pathways and mediate MT1-MMP-dependent invasion of cancer cells.

458 Therefore, a pro-tumorigenic role of *Kif13a* maybe its involvement in MT1-MMP trafficking to

459 the cell surface. KIF9 is mainly deleted rather than amplified across the TCGA database.

460 According to the Pathology Atlas, it is a favorable prognostic marker in renal and colorectal

461 cancers (Figure 10e and 10f). Thus, KIF9 may have an anti-tumorigenic potential for these

462 two cancer types. These data highlight that KIF13A and KIF9 may have cancer type-specific

463 roles, at least partly due to their roles in MT1-MMP intracellular trafficking. Chandrasekaran

464 et al. (Chandrasekaran et al., 2015) used cBioPortal to search for kinesin gene alterations in

465 TCGA. They reported that the *Kif13a* gene was amplified in more than 10% of patients

466 diagnosed with serous ovarian adenocarcinoma or urothelial bladder

467 carcinoma(Chandrasekaran et al., 2015). They also found that 12% of patients with clear

468 renal carcinoma had a homozygous deletion of the *Kif9* gene(Chandrasekaran et al., 2015).

469 These values were slightly different from our analysis of the TCGA database. The

470 discrepancies are likely due to the large number of data added to the database after

471 publication. Cho *et al.*(Cho et al., 2019) performed an integrated analysis of specific

472 kinesin's clinical significance, including KIF9, in low-grade glioma and glioblastoma. They

473 showed that high KIF9 expression is linked to cancer progression and significantly lower

474 survival probability, especially for patients diagnosed with glioblastoma(Cho et al., 2019).

475 Thus, the role of KIF9 may be cancer-specific.

476   In conclusion, we have identified KIF3A, KIF13A, and KIF9-v1 as the major KIFs that

477 traffic MT1-MMP vesicles in HT1080 cells. KIF3A and KIF13A collaborate and transport

478 MT1-MMP to the leading edge, while KIF9-v1 seems to compete with KIF13A and KIF3A by

479 trafficking MT1-MMP-containing vesicles to non-leading edge membrane structures. Our

480 findings revealed novel mechanisms of interplay between different KIFs, which contribute to

481 the understanding of vesicle transport mechanisms during cancer invasion.

482

483 **MATERIALS AND METHODS**

484 ***Plasmid constructs***

485   MT1-RFP in pSG5 vector (Stratagene) was generated as described previously (Itoh et al.,

486   2011). cDNAs encoding human KIF13A, KIF3A, KIF9-v1, KIF9-v2 and KIF1C were amplified

487   by PCR using a cDNA library from HT-1080 cells as template. The AcGFP was inserted at

488   the N-terminus of each KIFs with three glycine as linker. The mutants were constructed by

489   the overlap extension PCR method. KIF13A-GFP (forward primer for AcGFP: 5'-

490   TAGGAGCTCGGTACCGCCGCCACCATGGTGAGCAAGGGCG-3'; reverse primer: 5'-

491   CCATTCCACCTCCCTTGTACAGCTATCCATGC-3'; forward chimera primer for AcGFP-

492   KIF13A: 5'-TAGGAGCTCGGTACCGCCGCCACCATGGTGAGCGCAAGGGCG-3'; reverse

493   flanking primer: 5'-TAGCCCGGGTCACTTGTACAGCTCATCCATGC-3'). KIF3A-GFP

494   (forward flanking primer: 5'-

495   ATACGACTCACTATAGGGCGAATTCGAGCCACCATGGTGAGCAAGGGCGCC-3';

496   reverse primer: 5'-CGGCATTCCACCTCCCTTGTACACTCATCCATGCCGTG-3'; forward

497   chimera primer for AcGFP-KIF3A: 5'-

498   TACAAGGGAGGTGGAATGCCGATCGGTAAATCAGA-3'; flanking reverse primer: 5'-

499   CCTCTTCATCATCATCTTCC-3'), KIF9-v2 (forward flanking primer: 5'-

500   AATTCGAGCTCGGTACCCAGATCTGCCACCATGGTGAGCAAGGGCG-3'; reverse primer:

501   5'-CCCATTCCACCTCCCTTGTACAGCTCATCCATGCCG-3'; forward chimera primer for

502   AcGFP-KIF9-v2: 5'-ACAAGGGAGGTGGAATGGGTACTAGGAAAAAAGTTC-3'; flanking

503   reverse primer: 5'-AATAAGATCTGGATCCCCCTATTTTCTATGTGCCTGCTG-3') and

504   KIF1C-GFP (forward flanking primer: 5'-

505   AARRCGAGCTCGGTACCCGCCACCATGGTGAGCAAGGGCGCC-3'; reverse primer: 5'-

506   GCCATTCCACCTCCCTTGTACAGCTCATCCATGCCGTG-3'; forward chimera primer for

507   AcGFP-KIF1C: 5'-TACAAGGGAGGTGGAATGGCTGGTGCCTCGGTCAA-3'; flanking

508   reverse primer: 5'-AATAAGATCTGGATCCCCTCACACAGCTGCCCCACTCTC-3'). KIF9-v1-

509   GFP was generated by restriction enzyme cloning. KIF3A-HaloTag and KIF9-v2-HaloTag

510   were generated by sub-cloning KIF3A and KIF9-v2 into pHTN HaloTag CMV-neo

511   (Promega). KIF13A, KIF13A-GFP, KIF9-v1, KIF9-v2, KIF9-v1-GFP, KIF9-v2-GFP, KIF1C,

512   and KIF1C-GFP were subcloned into pSG5 vector.

513

Cell culture, transient transfection and siRNA treatment

HT-1080 human fibrosarcoma cells (ECACC) were cultured in Dulbecco's modified Eagle's medium (DMEM) (Lonza), containing 10% FBS (Gibco), penicillin/ streptomycin (P/S) (PAA). Rheumatoid arthritis synovial fibroblasts derived from three different patients were cultured in DMEM supplemented with 20% FBS and P/S (Miller et al., 2009). HT-1080 cells were transfected with plasmid constructs using Trans-IT2020 (Mirus Bio) according to the manufacturer's instructions. Gene silencing was performed by transfection of SMARTpool ON-TARGETplus siRNA (Dharmacon, Thermo Fisher, Waltham, US) using INTERFERin (Polyplus-transfection) according to the manufacturer's instructions. Non-targeting siRNA (NT siRNA) was also purchased from Dharmacon. Gene silencing effectiveness was tested by Western blotting (WB) or RT-PCR. Cells were subjected for the experiments after 72 hours of transfection.

526

SDS-PAGE and Western blotting

Cell lysates were prepared by directly dissolving in 1xSDS loading buffer containing 0.1% 2-mercaptoethanol. Cell lysates were subjected to SDS-PAGE and the proteins in the gel were transferred to a PBDF membrane using Trans-Blot Turbo Transfer System (Bio-Rad). After probing the membrane with the primary antibodies, the bands were visualised using fluorescently-labelled secondary antibodies (LI-COR). Membranes were scanned by Odyssey CLx imaging system (LI-COR). The band intensities were quantified by ImageJ software (National Institutes of Health). Actin or tubulin bands were used for normalisation. Mean band intensities were plotted using Prism (GraphPad software, Inc.) and statistical significance was calculated using either a parametric unpaired T test or a one-way ordinary ANOVA with Tuckey's multiple comparison test. The following primary antibodies were used: rabbit anti-MT1-MMP monoclonal antibody (clone EP1264Y, ab51074, abcam), mouse anti-MT1-MMP monoclonal antibody (clone 222-1D8), rabbit anti-KIF1C polyclonal antibody (ab72238, abcam), rabbit anti-KIF3A polyclonal antibody (ab11259, abcam), mouse anti-

541 actin monoclonal antibody (clone C4, sc47778, Santa Cruz), mouse anti-tubuline antibody

542 (clone B-7, sc5286, Santa Crutz). The following secondary antibodies were used: IRDye

543 680RD goat anti-mouse IgG (H + L) (926-68070, LI-COR), IRDye 800CW goat ant-rabbit

544 IgG (H + L) (926-32211, LI-COR).

545

546 ***RT-PCR***

547 Total RNA was isolated using the RNAqueous Micro kit (Invitrogen) according to the

548 manufacturer's instructions. RNA was reversed-transcribed using the High Capacity cDNA

549 Reverse Transcription kit from AB applied Biosciences (Thermo Fisher). Resulted cDNA was

550 used as a template for PCR using the Dream Taq Polymerase (Thermo Fisher). GADPH

551 was used as housekeeping gene. The following primers were used: KIF13A (forward: 5'-

552 TTTCCAGTAGGAGGAGTC-3'; reverse: 5'-AAGTTGTTGCGGTGAAGG-3'), KIF3A (forward:

553 5'-TGCAAAGTCAGAGATGGC-3'; reverse: AGCTGCCATTCTCCTATG-3'), KIF9 (forward:

554 5'-CCCGGACCTTATCAGAGGAAAAG-3'; reverse (v1): 5'-GGTGTCGGGCCTGAGTGG-3';

555 reverse (v2): 5'-GGATGGGACAAGCTGGGTC-3'), KIF1C (forward: 5'-

556 TTCCAGCCCAAAAAGCAC-3'; reverse: 5'-CGGACCTTCTCTCTCATC-3'), KIF5B (forward:

557 5'-GCTACAAGAGTTAAAAAGAGTGCT-3'; reverse: 5'-TCACACTTGTTTGCCTCCTCCAG-

558 3'), MT1-MMP (forward: 5'- GGGACCTACGTACCCACACA; reverse: 5'-

559 TAGCGCTTCCTTCGAACATT-3') AND GADPH (forward: 5'-

560 TTCACCACCATGGAGAAGGC-3'; reverse: 5'- GGTCCCTCCGATGCCTGC-3'). RT-PCR

561 gels were quantified by Fiji using the same protocol described above for the quantification of

562 WB gels. GADPH bands were used for normalisation.

563

564 ***Gelatin film degradation assay***

565 Fluorescently-labelled gelatin coated coverslips were prepared as described

566 previously (Evans and Itoh, 2007; Itoh et al., 2006). Cells were cultured atop of the gelatin-

567 coated coverslips for 2-15 hours, depending on the assay, in the presence or absence of

568 GM6001 (10 μM) (Elastin Products Company), TIMP-1 (200 nM), or DX-2400 (200 nM).

569   TIMP-1 was a gift from Prof Gillian Murphy (University of Cambridge), and DX-2400 was a

570   gift from Dyax Corp. Cells were then fixed in 4% formaldehyde (Sigma Aldrich) in PBS for 15

571   minutes and stained with DAPI (Sigma-Aldrich). Images were acquired with a Nikon

572   microscope with using the 10X dry lens (NA = 0.3) on a Nikon TE2000-E microscope

573   equipped with an ORCA-ER CCD camera (Hammamatsu Photonics) operated by Volocity

574   Acquisition module software (Improvision). Gelatin film degradation was quantified using Fiji.

575   Area of degradation was calculated using the gelatin fluorescence image which was

576   converted to greyscale and thresholded. The threshold was set the same for all the pictures

577   analysed, in order to have an objective mean of analysis. Area and area fraction were

578   measured. The DAPI-stained corresponding image was converted to a binary image in order

579   to count the number of cells in the microscopic field. The degraded area per cell was

580   calculated as follow:

$$\text{Degraded Area per cell } (\mu m^2) = \frac{\text{Total Degraded Area}}{\text{Number of Cells}}$$

581   Mean degraded areas were plotted using Prism and statistical significance was calculated

582   using one-way ordinary ANOVA with Tuckey's multiple comparison test.

583

584   ***Collagen film degradation assay***

585   Collagen film degradation was carried out as described previously (Evans and Itoh,

586   2007; Itoh et al., 2006). Briefly, PureCol (bovine collagen type-I, Advanced Biomatrix) and

587   Cellmatrix type I-A collagen (Nitta Gelatin) were mixed in the ratio 1:1. This mixture was

588   neutralised and diluted to a 2 mg/ml. 12-well multi well plates were coated with 100 µl

589   collagen solution/well and set for gelation. Cells were cultured on the collagen film for 72

590   hours in the presence or absence of GM6001 (10 µM), TIMP-1 (200 nM), or DX-2400 (200

591   nM). Cells were removed extensively by trypsin/EDTA (Lonza) and the remaining collagen

592   layer was fixed with 4% formaldehyde in PBS and stained with R-250 Coomassie Brilliant

593   Blue (Thermo Fisher). Representative images were acquired using the 10X dry lens (NA =

594   0.3) on the Nikon TE2000-E microscope equipped with an ORCA-ER CCD camera

595   (Hammamatsu Photonics) operated by Volocity Acquisition module software (Improvision,

596   PerkinElmer). Collagen degradation was quantified using Fiji by measuring the integrated

597   density of the collagen layer. Mean results were plotted using Prism and statistical

598   significance was calculated using one-way ordinary ANOVA with Tuckey's multiple

599   comparison test.

600

601   ***Zymography***

602   Gelatin zymography was conducted as reported previously (Evans and Itoh, 2007; Itoh et al.,

603   2006). Enzyme activity was visualised directly on the gels as negative staining bands with

604   Coomassie Blue. Pro-MMP-2 (P), intermediate MMP-2 (I) and active MMP-2 (A) bands were

605   quantified using Fiji. The percentage of processed pro-MMP-2 over the total was calculated

606   as   follow:

$$\frac{Area\ Peaks\ (I + A)}{Area\ Peaks\ (\ P + I + A)} * 100$$

607

608   ***Cell Surface biotinylation***

609   Surface biotinylation was carried out using Sulfo-NHS-biotin (Thermo Fisher) as described

610   previously(Itoh et al., 2001). Cells were cultured to confluency, and cell surface proteins

611   were labelled with sulfo-NHS-biotin (Thermo-Fischer), followed by affinity precipitation of

612   biotinylated molecules by streptavidin-conjugated Dyna beads (Thermo Fisher). The eluted

613   samples were subjected to Western Blotting analyses using rabbit monoclonal anti-MT1-

614   MMP antibody.

615

616   ***Indirect immunofluorescent staining***

617   Cells cultured atop of un-labelled or fluorescently labelled gelatin were fixed with 4% (v/v)

618   formaldehyde in PBS for 5 min and blocked with 3% (w/v) BSA, 5% (v/v) goat serum in TBS

619   (blocking solution) for 1 hour at room temperature (RT). Cells were then incubated with

620   primary antibodies in blocking solution. The cells were further probed by Alexa488-

23

621   conjugated goat anti-mouse IgG (Molecular Probes), DyLight650-conjugated goat anti-rabbit

622   IgG (Thermo Scientific), Alexa568-conjugated Phalloidin (Molecular Probes, Thermo Fisher)

623   or DAPI. The following primary antibodies were used for staining: rabbit anti-MT1-MMP

624   monoclonal antibody (clone EP1264Y, abcam), mouse anti-human β1 integrin monoclonal

625   antibody (clone 12G10, Millipore).

626

627   ***Trans-well invasion assay***

628   Trans-well invasion assay was performed as previously described(Palmisano and Itoh,

629   2010). Briefly, a 24-well insert with an 8-μm-pore membrane Trans-wells (VWR International

630   Ltd) was coated with 50 μl of CellMatrix/PureCol collagen mixture (1:1, 2 mg/ml), incubated

631   at 37°C for 1 hour to set the collagen and dried overnight at RT. Cells (2×10^4/well) were

632   seeded in the upper chamber and further cultured for 18 hours. Lower chamber media

633   contained 10% FBS while upper chamber media was serum free. Invaded cells were stained

634   with DAPI, imaged with fluorescence microscopy, and analyzed by Volocity software.

635

636   ***Microcarrier beads invasion assay***

637   Microcarrier beads invasion assay was carried out as described previously

638   (Palmisano and Itoh, 2010). Cells were attached to gelatin-coated Cytodex 3 microcarrier

639   beads (VWR) by preparing a cell/bead suspension which was incubated on a shaker for 6

640   hours at 37°C. Beads coated with cells were suspended in neutralised Cellmatrix collagen

641   (final concentration 2 mg/ml) and incubated overnight in the presence or absence of

642   GM6001 (10 μM). Invasion was analysed as the distance between a cell nucleus and the

643   surface of the bead using the line tool of ImageJ. Migrated distances were calculated for

644   fifty cells per treatment. Mean migrated distances were plotted using Prism and statistical

645   significance was calculated using one-way ordinary ANOVA with Tuckey's multiple

646   comparison test.

647

648   ***Wound-healing assay***

24

649   Ibidi Culture-Inserts (Ibidi) consisting of two reservoirs separated by a 500-µm-width

650 wall was placed in each well of a 24-well plate and six inserts were used for each treatment.

651 Cells were seeded in the two reservoirs of the inserts and incubated until confluence. After

652 the inserts were gently removed, cells were further cultured for 6 hours. Pictures were taken

653 immediately after the inserts were removed and at the 6-hour time point. To measure the

654 percentage of wound closure, ImageJ was employed. For each condition, the ROI

655 corresponding to the initial wound-gap (ROI-I) and the one, delimited by the migration front

656 after 6 hours of incubation (ROI-F), were calculated. The percentage of wound closure was

657 calculated as follow:

$$\text{Wound Closure (\%)} = \frac{(\text{ROI} - \text{I}) - (\text{ROI} - \text{F})}{\text{ROI} - \text{I}} * 100$$

658 Mean percentages were plotted using Prism and statistical significance was calculated using

659 one-way ordinary ANOVA with Tuckey's multiple comparison test.

660

661 ***Live cell imaging***

662 Cells were transfected with GFP-tagged KIFs, Halo-tagged KIFs and MT1-RFP. After 36

663 hours they were seeded at a density of 4×10^3/well on gelatin-coated glass-bottomed 8-well

664 chambers (Ibidi). After 12 hours, live images were acquired by either confocal laser scanning

665 microscopy or total internal reflection fluorescence (TIRF) microscopy (details specified

666 below). Both microscopes were equipped with an environmental chamber to maintain

667 temperature at 37°C and CO_2 at 5%. Time-lapse images were acquired every 3 to 30

668 seconds, depending on the experiment.

669

670 ***Image acquisition***

671 All widefield images were captured on an inverted Nikon TE2000-E widefield microscope

672 with Volocity Acquisition software (PerkinElmer). These objective lenses were used: 4X

673 objective lens (Plan Fluor 4X/NA 0.13), 10X objective lens (UPLSAPO 10X/NA 0.30 DIC),

674 and 20X objective lens (UPLSAPO 20X/NA 0.45). Confocal laser scanning microscopy

675 imaging was performed on a PerkinElmer Spinning Disk Confocal Microscope based on a

676 Nikon TE 2000-U Eclipse motorized inverted microscope with DIC optics. A 60X objective

677 lens was used: 60X (Plan Apo 60×/NA 1.40). Volocity software (PerkinElmer, Coventry, UK)

678 was used for Acquisition. For TIRFM an Olympus microscope in TIRF mode (CellTIRF-4Line

679 system; Olympus), equipped with an EMCCD camera (Evolve) was used. A 150X objective

680 lens was used (UPLSAPO 150 X/ NA 1.45).

681

682 ***Data analysis***

683 To measure the amount of either β1 integrin and MT1-MMP at the substrate-

684 attachment side, the corresponding fluorescence intensities (FIs) were measured by ImageJ.

685 TIRF images were analysed by defining a region of interest (ROI), corresponding to the cell

686 body (ROI-CB), and a rectangular ROI in the background (ROI-B). FIs were calculated as

687 follow:

$$FI = \ FI(ROI - CB) - FI(ROI - B)$$

688 30 cells were analysed for each condition. ROI-B dimension and position was kept the same

689 throughout the course of the analysis. Mean FIs were plotted using Prism and statistical

690 significance was calculated using one-way ordinary ANOVA with Tuckey's multiple

691 comparison test.

692 To measure the overall amount of MT1-MMP on the cell surface of HT-1080 cells,

693 FIs were analysed by Volocity measurement module software. Extended focus images of

694 HT-1080 cells stained for cell surface endogenous MT1-MMP, captured by spinning disk

695 confocal microscope were used. Thirty cells were analysed for each condition. Mean FIs

696 were plotted using Prism and statistical significance was calculated using one-way ordinary

697 ANOVA with Tuckey's multiple comparison test.

698 Co-localisation between GFP-tagged KIFs and MT1-RFP was quantified using the

699 Coloc 2 plugin in Fiji, which calculates Pearson's correlation coefficients (PCCs). This

700 procedure was used on two-colour channel images of cells cultured on 2D matrices and on

701 two-colour channel stacks of cells cultured in 3D collagen matrices. Mean PCCs were

702 plotted using Prism and statistical significance was calculated using one-way ordinary

703 ANOVA with Tuckey's multiple comparison test.

704   Tracking of MT1-RFP-containing vesicles trafficked by GFP-tagged KIFs was

705 performed using the Track Mate plugin (Tinevez et al., 2017) in Fiji. Vesicles were identified

706 using the LoG detector and their diameter was estimated at 1.5 µm. Tracking was performed

707 by Simple LAP Tracker using 2 µm as linking and gap-closing maximum distances. The gap-

708 closing maximum frame gap was set at 2. Mean velocities and vesicle diameters were

709 calculated automatically by the plugin. Data were plotted using Prism and statistical

710 significance was calculated by a parametric unpaired T test or a one-way ordinary ANOVA

711 with Tuckey's multiple comparison test.

712   To analyse genomic alterations of Kif13a, Kif3a and Kif9 genes in cancer, we

713 employed cBioPortal (Cerami et al., 2012; Gao et al., 2013) (https://www.cbioportal.org). The

714 Cancer Genome Atlas (TCGA) PanCancer Atlas studies were selected to visualise and

715 analyse Kif13a, Kif3a and Kif9 gene alterations. The Human Protein Atlas

716 (https://www.proteinatlas.org) was used to check whether Kif13a Kif3a or Kif9 genes were

717 prognostic markers for specific cancer types.

718

719 **ACKNOWLEDGEMENT**

726

727 **REFERENCES**

728 Castro-Castro, A., V. Marchesin, P. Monteiro, C. Lodillinsky, C. Rosse, and P. Chavrier.
729   2016. Cellular and Molecular Mechanisms of MT1-MMP-Dependent Cancer Cell
730   Invasion. *Annu Rev Cell Dev Biol*. 32:555-576.

731 Cerami, E., J. Gao, U. Dogrusoz, B.E. Gross, S.O. Sumer, B.A. Aksoy, A. Jacobsen, C.J.
732   Byrne, M.L. Heuer, E. Larsson, Y. Antipin, B. Reva, A.P. Goldberg, C. Sander, and
733   N. Schultz. 2012. The cBio cancer genomics portal: an open platform for exploring
734   multidimensional cancer genomics data. *Cancer Discov*. 2:401-404.
735 Chan, K.M., H.L. Wong, G. Jin, B. Liu, R. Cao, Y. Cao, K. Lehti, K. Tryggvason, and Z.
736   Zhou. 2012. MT1-MMP inactivates ADAM9 to regulate FGFR2 signaling and calvarial
737   osteogenesis. *Dev Cell*. 22:1176-1190.
738 Chandrasekaran, G., P. Tatrai, and F. Gergely. 2015. Hitting the brakes: targeting
739   microtubule motors in cancer. *Br J Cancer*. 113:693-698.
740 Cho, S.Y., S. Kim, G. Kim, P. Singh, and D.W. Kim. 2019. Integrative analysis of KIF4A, 9,
741   18A, and 23 and their clinical significance in low-grade glioma and glioblastoma. *Sci
742   Rep*. 9:4599.
743 Cornfine, S., M. Himmel, P. Kopp, K. El Azzouzi, C. Wiesner, M. Kruger, T. Rudel, and S.
744   Linder. 2011. The kinesin KIF9 and reggie/flotillin proteins regulate matrix
745   degradation by macrophage podosomes. *Mol Biol Cell*. 22:202-215.
746 Devy, L., L. Huang, L. Naa, N. Yanamandra, H. Pieters, N. Frans, E. Chang, Q. Tao, M.
747   Vanhove, A. Lejeune, R. van Gool, D.J. Sexton, G. Kuang, D. Rank, S. Hogan, C.
748   Pazmany, Y.L. Ma, S. Schoonbroodt, A.E. Nixon, R.C. Ladner, R. Hoet, P.
749   Henderikx, C. Tenhoor, S.A. Rabbani, M.L. Valentino, C.R. Wood, and D.T.
750   Dransfield. 2009. Selective inhibition of matrix metalloproteinase-14 blocks tumor
751   growth, invasion, and angiogenesis. *Cancer research*. 69:1517-1526.
752 Endo, K., T. Takino, H. Miyamori, H. Kinsen, T. Yoshizaki, M. Furukawa, and H. Sato. 2003.
753   Cleavage of syndecan-1 by membrane type matrix metalloproteinase-1 stimulates
754   cell migration. *J Biol Chem*. 278:40764-40770.
755 Evans, R.D., and Y. Itoh. 2007. Analyses of MT1-MMP activity in cells. *Methods Mol Med*.
756   135:239-249.
757 Ferrari, R., G. Martin, O. Tagit, A. Guichard, A. Cambi, R. Voituriez, S. Vassilopoulos, and P.
758   Chavrier. 2019. MT1-MMP directs force-producing proteolytic contacts that drive
759   tumor cell invasion. *Nat Commun*. 10:4886.
760 Frittoli, E., A. Palamidessi, A. Disanza, and G. Scita. 2011. Secretory and endo/exocytic
761   trafficking in invadopodia formation: the MT1-MMP paradigm. *European journal of
762   cell biology*. 90:108-114.
763 Gao, J., B.A. Aksoy, U. Dogrusoz, G. Dresdner, B. Gross, S.O. Sumer, Y. Sun, A. Jacobsen,
764   R. Sinha, E. Larsson, E. Cerami, C. Sander, and N. Schultz. 2013. Integrative
765   analysis of complex cancer genomics and clinical profiles using the cBioPortal. *Sci
766   Signal*. 6:pl1.
767 Gifford, V., and Y. Itoh. 2019. MT1-MMP-dependent cell migration: proteolytic and non-
768   proteolytic mechanisms. *Biochem Soc Trans*.
769 Hirokawa, N. 2000. Stirring up development with the heterotrimeric kinesin KIF3. *Traffic*.
770   1:29-34.
771 Hirokawa, N., Y. Noda, Y. Tanaka, and S. Niwa. 2009. Kinesin superfamily motor proteins
772   and intracellular transport. *Nat Rev Mol Cell Biol*. 10:682-696.
773 Hirokawa, N., and Y. Tanaka. 2015. Kinesin superfamily proteins (KIFs): Various functions
774   and their relevance for important phenomena in life and diseases. *Exp Cell Res*.
775   334:16-25.
776 Holmbeck, K., P. Bianco, S. Yamada, and H. Birkedal-Hansen. 2004. MT1-MMP: a tethered
777   collagenase. *J Cell Physiol*. 200:11-19.
778 Idzko, M., M. Laut, E. Panther, S. Sorichter, T. Durk, J.W. Fluhr, Y. Herouy, M.
779   Mockenhaupt, D. Myrtek, P. Elsner, and J. Norgauer. 2004. Lysophosphatidic acid
780   induces chemotaxis, oxygen radical production, CD11b up-regulation, Ca2+
781   mobilization, and actin reorganization in human eosinophils via pertussis toxin-
782   sensitive G proteins. *J Immunol*. 172:4480-4485.
783 Infante, E., A. Castagnino, R. Ferrari, P. Monteiro, S. Aguera-Gonzalez, P. Paul-Gilloteaux,
784   M.J. Domingues, P. Maiuri, M. Raab, C.M. Shanahan, A. Baffet, M. Piel, E.R.
785   Gomes, and P. Chavrier. 2018. LINC complex-Lis1 interplay controls MT1-MMP

786   matrix digest-on-demand response for confined tumor cell migration. *Nat Commun*.
787   9:2443.
788   Itoh, Y. 2015. Membrane-type matrix metalloproteinases: Their functions and regulations.
789   *Matrix Biol*. 44-46:207-223.
790   Itoh, Y., N. Ito, H. Nagase, R.D. Evans, S.A. Bird, and M. Seiki. 2006. Cell surface
791   collagenolysis requires homodimerization of the membrane-bound collagenase MT1-
792   MMP. *Mol Biol Cell*. 17:5390-5399.
793   Itoh, Y., R. Palmisano, N. Anilkumar, H. Nagase, A. Miyawaki, and M. Seiki. 2011.
794   Dimerization of MT1-MMP during cellular invasion detected by fluorescence
795   resonance energy transfer. *Biochem J*. 440:319-326.
796   Itoh, Y., A. Takamura, N. Ito, Y. Maru, H. Sato, N. Suenaga, T. Aoki, and M. Seiki. 2001.
797   Homophilic complex formation of MT1-MMP facilitates proMMP-2 activation on the
798   cell surface and promotes tumor cell invasion. *EMBO J*. 20:4782-4793.
799   Jiang, A., K. Lehti, X. Wang, S.J. Weiss, J. Keski-Oja, and D. Pei. 2001. Regulation of
800   membrane-type matrix metalloproteinase 1 activity by dynamin-mediated
801   endocytosis. *Proc Natl Acad Sci U S A*. 98:13693-13698.
802   Jin, G., F. Zhang, K.M. Chan, H.L. Xavier Wong, B. Liu, K.S. Cheah, X. Liu, C. Mauch, D.
803   Liu, and Z. Zhou. 2011. MT1-MMP cleaves Dll1 to negatively regulate Notch
804   signalling to maintain normal B-cell development. *EMBO J*. 30:2281-2293.
805   Kajita, M., Y. Itoh, T. Chiba, H. Mori, A. Okada, H. Kinoh, and M. Seiki. 2001. Membrane-
806   type 1 matrix metalloproteinase cleaves CD44 and promotes cell migration. *J Cell
807   Biol*. 153:893-904.
808   Kaneko, K., R.O. Williams, D.T. Dransfield, A.E. Nixon, A. Sandison, and Y. Itoh. 2016.
809   Selective Inhibition of Membrane Type 1 Matrix Metalloproteinase Abrogates
810   Progression of Experimental Inflammatory Arthritis: Synergy With Tumor Necrosis
811   Factor Blockade. *Arthritis Rheumatol*. 68:521-531.
812   Koshikawa, N., D. Hoshino, H. Taniguchi, T. Minegishi, T. Tomari, S.O. Nam, M. Aoki, T.
813   Sueta, T. Nakagawa, S. Miyamoto, K. Nabeshima, A.M. Weaver, and M. Seiki. 2015.
814   Proteolysis of EphA2 Converts It from a Tumor Suppressor to an Oncoprotein.
815   *Cancer research*. 75:3327-3339.
816   Le Borgne, R., and B. Hoflack. 1998. Protein transport from the secretory to the endocytic
817   pathway in mammalian cells. *Biochimica et biophysica acta*. 1404:195-209.
818   Lehti, K., J. Lohi, M.M. Juntunen, D. Pei, and J. Keski-Oja. 2002. Oligomerization through
819   hemopexin and cytoplasmic domains regulates the activity and turnover of
820   membrane-type 1 matrix metalloproteinase. *J Biol Chem*. 277:8440-8448.
821   Majkowska, I., Y. Shitomi, N. Ito, N.S. Gray, and Y. Itoh. 2017. Discoidin domain receptor 2
822   mediates collagen-induced activation of membrane-type 1 matrix metalloproteinase
823   in human fibroblasts. *J Biol Chem*. 292:6633-6643.
824   Marchesin, V., A. Castro-Castro, C. Lodillinsky, A. Castagnino, J. Cyrta, H. Bonsang-Kitzis,
825   L. Fuhrmann, M. Irondelle, E. Infante, G. Montagnac, F. Reyal, A. Vincent-Salomon,
826   and P. Chavrier. 2015. ARF6-JIP3/4 regulate endosomal tubules for MT1-MMP
827   exocytosis in cancer invasion. *J Cell Biol*. 211:339-358.
828   Miller, M.C., H.B. Manning, A. Jain, L. Troeberg, J. Dudhia, D. Essex, A. Sandison, M. Seiki,
829   J. Nanchahal, H. Nagase, and Y. Itoh. 2009. Membrane type 1 matrix
830   metalloproteinase is a crucial promoter of synovial invasion in human rheumatoid
831   arthritis. *Arthritis Rheum*. 60:686-697.
832   Nakagawa, T., M. Setou, D. Seog, K. Ogasawara, N. Dohmae, K. Takio, and N. Hirokawa.
833   2000. A novel motor, KIF13A, transports mannose-6-phosphate receptor to plasma
834   membrane through direct interaction with AP-1 complex. *Cell*. 103:569-581.
835   Ohuchi, E., K. Imai, Y. Fujii, H. Sato, M. Seiki, and Y. Okada. 1997. Membrane type 1 matrix
836   metalloproteinase digests interstitial collagens and other extracellular matrix
837   macromolecules. *J Biol Chem*. 272:2446-2451.
838   Palmisano, R., and Y. Itoh. 2010. Analysis of MMP-dependent cell migration and invasion.
839   *Methods Mol Biol*. 622:379-392.

840   Pedersen, N.M., E.M. Wenzel, L. Wang, S. Antoine, P. Chavrier, H. Stenmark, and C.
841   Raiborg. 2020. Protrudin-mediated ER-endosome contact sites promote MT1-MMP
842   exocytosis and cell invasion. *J Cell Biol.* 219.
843   Perez Bay, A.E., R. Schreiner, F. Mazzoni, J.M. Carvajal-Gonzalez, D. Gravotta, E. Perret,
844   G. Lehmann Mantaras, Y.S. Zhu, and E.J. Rodriguez-Boulan. 2013. The kinesin
845   KIF16B mediates apical transcytosis of transferrin receptor in AP-1B-deficient
846   epithelia. *EMBO J.* 32:2125-2139.
847   Planchon, D., E. Rios Morris, M. Genest, F. Comunale, S. Vacher, I. Bieche, E.V. Denisov,
848   L.A. Tashireva, V.M. Perelmuter, S. Linder, P. Chavrier, S. Bodin, and C. Gauthier-
849   Rouviere. 2018. MT1-MMP targeting to endolysosomes is mediated by upregulation
850   of flotillins. *J Cell Sci.* 131.
851   Poincloux, R., F. Lizárraga, and P. Chavrier. 2009. Matrix invasion by tumour cells: a focus
852   on MT1-MMP trafficking to invadopodia. *J Cell Sci.* 122:3015-3024.
853   Remacle, A., G. Murphy, and C. Roghi. 2003. Membrane type I-matrix metalloproteinase
854   (MT1-MMP) is internalised by two different pathways and is recycled to the cell
855   surface. *J Cell Sci.* 116:3905-3916.
856   Rozanov, D.V., E. Hahn-Dantona, D.K. Strickland, and A.Y. Strongin. 2004. The low density
857   lipoprotein receptor-related protein LRP is regulated by membrane type-1 matrix
858   metalloproteinase (MT1-MMP) proteolysis in malignant cells. *J Biol Chem.* 279:4260-
859   4268.
860   Sabeh, F., I. Ota, K. Holmbeck, H. Birkedal-Hansen, P. Soloway, M. Balbin, C. Lopez-Otin,
861   S. Shapiro, M. Inada, S. Krane, E. Allen, D. Chung, and S.J. Weiss. 2004. Tumor cell
862   traffic through the extracellular matrix is controlled by the membrane-anchored
863   collagenase MT1-MMP. *J Cell Biol.* 167:769-781.
864   Sabeh, F., R. Shimizu-Hirota, and S.J. Weiss. 2009. Protease-dependent versus -
865   independent cancer cell invasion programs: three-dimensional amoeboid movement
866   revisited. *J Cell Biol.* 185:11-19.
867   Sato, H., T. Takino, Y. Okada, J. Cao, A. Shinagawa, E. Yamamoto, and M. Seiki. 1994. A
868   matrix metalloproteinase expressed on the surface of invasive tumour cells. *Nature.*
869   370:61-65.
870   Seiki, M. 2003. Membrane-type 1 matrix metalloproteinase: a key enzyme for tumor
871   invasion. *Cancer Lett.* 194:1-11.
872   Shakya, S., P. Sharma, A.M. Bhatt, R.A. Jani, C. Delevoye, and S.R. Setty. 2018. Rab22A
873   recruits BLOC-1 and BLOC-2 to promote the biogenesis of recycling endosomes.
874   *EMBO Rep.* 19.
875   Sithu, S.D., W.R. English, P. Olson, D. Krubasik, A.H. Baker, G. Murphy, and S.E. D'Souza.
876   2007. Membrane-type 1-matrix metalloproteinase regulates intracellular adhesion
877   molecule-1 (ICAM-1)-mediated monocyte transmigration. *J Biol Chem.* 282:25010-
878   25019.
879   Stanton, H., J. Gavrilovic, S.J. Atkinson, M.P. d'Ortho, K.M. Yamada, L. Zardi, and G.
880   Murphy. 1998. The activation of ProMMP-2 (gelatinase A) by HT1080 fibrosarcoma
881   cells is promoted by culture on a fibronectin substrate and is concomitant with an
882   increase in processing of MT1-MMP (MMP-14) to a 45 kDa form. *J Cell Sci.*
883   111:2789-2798.
884   Sugiyama, N., E. Gucciardo, O. Tatti, M. Varjosalo, M. Hyytiainen, M. Gstaiger, and K. Lehti.
885   2013. EphA2 cleavage by MT1-MMP triggers single cancer cell invasion via
886   homotypic cell repulsion. *J Cell Biol.* 201:467-484.
887   Taniwaki, K., H. Fukamachi, K. Komori, Y. Ohtake, T. Nonaka, T. Sakamoto, T. Shiomi, Y.
888   Okada, T. Itoh, S. Itohara, M. Seiki, and I. Yana. 2007. Stroma-derived matrix
889   metalloproteinase (MMP)-2 promotes membrane type 1-MMP-dependent tumor
890   growth in mice. *Cancer research.* 67:4311-4319.
891   Teng, J., T. Rai, Y. Tanaka, Y. Takei, T. Nakata, M. Hirasawa, A.B. Kulkarni, and N.
892   Hirokawa. 2005. The KIF3 motor transports N-cadherin and organizes the developing
893   neuroepithelium. *Nat Cell Biol.* 7:474-482.

894   Thapa, N., and R.A. Anderson. 2017. PLD and PA Take MT1-MMP for a Metastatic Ride.
895   *Dev Cell*. 43:117-119.
896   Tinevez, J.Y., N. Perry, J. Schindelin, G.M. Hoopes, G.D. Reynolds, E. Laplantine, S.Y.
897   Bednarek, S.L. Shorte, and K.W. Eliceiri. 2017. TrackMate: An open and extensible
898   platform for single-particle tracking. *Methods*. 115:80-90.
899   Uhlen, M., C. Zhang, S. Lee, E. Sjostedt, L. Fagerberg, G. Bidkhori, R. Benfeitas, M. Arif, Z.
900   Liu, F. Edfors, K. Sanli, K. von Feilitzen, P. Oksvold, E. Lundberg, S. Hober, P.
901   Nilsson, J. Mattsson, J.M. Schwenk, H. Brunnstrom, B. Glimelius, T. Sjoblom, P.H.
902   Edqvist, D. Djureinovic, P. Micke, C. Lindskog, A. Mardinoglu, and F. Ponten. 2017.
903   A pathology atlas of the human cancer transcriptome. *Science*. 357.
904   Wang, Y., and M.A. McNiven. 2012. Invasive matrix degradation at focal adhesions occurs
905   via protease recruitment by a FAK-p130Cas complex. *J Cell Biol*. 196:375-385.
906   Wang, Z., F. Zhang, J. He, P. Wu, L.W.R. Tay, M. Cai, W. Nian, Y. Weng, L. Qin, J.T.
907   Chang, L.B. McIntire, G. Di Paolo, J. Xu, J. Peng, and G. Du. 2017. Binding of PLD2-
908   Generated Phosphatidic Acid to KIF5B Promotes MT1-MMP Surface Trafficking and
909   Lung Metastasis of Mouse Breast Cancer Cells. *Dev Cell*. 43:186-197 e187.
910   Wiesner, C., J. Faix, M. Himmel, F. Bentzien, and S. Linder. 2010. KIF5B and KIF3A/KIF3B
911   kinesins drive MT1-MMP surface exposure, CD44 shedding, and extracellular matrix
912   degradation in primary macrophages. *Blood*. 116:1559-1569.
913   Wolf, K., M. Te Lindert, M. Krause, S. Alexander, J. Te Riet, A.L. Willis, R.M. Hoffman, C.G.
914   Figdor, S.J. Weiss, and P. Friedl. 2013. Physical limits of cell migration: control by
915   ECM space and nuclear deformation and tuning by proteolysis and traction force. *J*
916   *Cell Biol*. 201:1069-1084.
917   Wolf, K., Y.I. Wu, Y. Liu, J. Geiger, E. Tam, C. Overall, M.S. Stack, and P. Friedl. 2007.
918   Multi-step pericellular proteolysis controls the transition from individual to collective
919   cancer cell invasion. *Nat Cell Biol*. 9:893-904.
920   Woskowicz, A.M., S.A. Weaver, Y. Shitomi, N. Ito, and Y. Itoh. 2013. MT-LOOP-dependent
921   localization of membrane type I matrix metalloproteinase (MT1-MMP) to the cell
922   adhesion complexes promotes cancer cell invasion. *J Biol Chem*. 288:35126-35137.
923

924

925 **FIGURE LEGENDS**

926 **Figure 1. Knockdown of KIF13A, KIF3A, KIF9 and KIF1C alters MT1-MMP-mediated**
927 **cell functions on the cell surface.**

928 **a.** HT-1080 cells were transfected with the indicated siRNAs and subjected to gelatin film
929 degradation assay in the presence or absence of GM6001 (10 μM). Scale bars are 130 μm.
930 Quantification of the degradation area (μm^2) per cell in HT-1080 cells transfected with the
931 indicated siRNAs was show as a graph (right panel). Data are presented as the mean of
932 fifteen independent microscopic fields of view and are representative of five independent
933 experiments. One-way ordinary Anova with Tuckey's multiple comparisons test. Data are
934 shown as mean ± SD. ****$P < 0.0001$.

935 **b.** HT-1080 cells were transfected with the indicated siRNAs and subjected to collagen film
936 degradation assay in the presence or absence of GM6001 (10 μM). Scale bars are 130 μm.
937 Quantification of the integrated density of the collagen layer in HT-1080 cells transfected
938 with the indicated siRNAs was shown as a graph (right panel). Data are presented as the
939 mean of eight independent microscopic fields of view and are representative of five
940 independent experiments. One-way ordinary Anova with Tuckey's multiple comparisons test.
941 Data are shown as mean ± SD. ****$P < 0.0001$; *$P < 0.05$.

942 **c.** HT-1080 cells transfected with the indicated siRNAs were cultivated in the presence or
943 absence of collagen I (100 μg/ml) for 24 h. Culture media were analysed by zymography
944 (Zymo) for proMMP-2 activation. Cell lysates were subjected to Western blotting using
945 antibodies for MT1-MMP Hpx domain and tubulin. Arrows point bands of interest. ProMMP-
946 2, 68 kDa proMMP-2; Intermediate, 65 kDa intermediate form; Active form, 62 kDa active
947 MMP-2. Quantification of the percentage of MMP-2 processed forms over the total was
948 shown as a graph (middle panel). Top panel shows processed MMP-2 without collagen
949 stimulation, and the bottom panel shows the MMP-2 activation upon collagen stimulation.
950 Quantification of the 45 kDa MT1-MMP processed forms (%) upon collagen stimulation was
951 shown as a graph (right panel). Data are calculated from five independent experiments.
952 One-way ordinary Anova with Tuckey's multiple comparisons test. Data are presented as
953 mean of five blots representative of five independent experiments. One-way ordinary Anova
954 with Tuckey's multiple comparisons test. Data are shown as mean ± SD. ****$P < 0.0001$; **P
955 < 0.01. n.s., non-significant.

956 **d.** Efficiency of KIF knockdown was assessed by Western blotting for KIF1C and KIF3A and
957 by RT-PCR for KIF13A, KIF9v1-v3. Effect of KIF knockdown on MT1-MMP mRNA level was
958 also examined. Quantification data were shown as a graph. Western blot band intensities
959 were normalized with Actin band intensities and mRNA normalized with the one for GAPDH.

960   **e**. HT1080 cells transfected with siRNA for KIF5B were subjected to gelatin film degradation

961   assay. Top panel shows representative images from each treatment as indicated. Bottom

962   left panel shows a quantitative data as degradation area per cells. Data is shown as mean ±

963   SD (n=12). n.s., non-significant. Bottom right panel shows a quantitative data of KIF5B

964   measured by Western blot. Data are presented as mean of three blots representative of

965   three independent experiments.

966

967   **Figure 2. Knockdown of KIF13A, KIF3A, KIF9 and KIF1C modifies MT1-MMP**

968   **localisation at the substrate-attachment side.**

969   **a.** HT-1080 cells were transfected with the indicated siRNAs subjected to cell surface

970   biotinylation. Proteins eluted from the streptavidin beads were analysed by Western blot

971   using anti-Loop MT1-MMP antibody. Whole cell lysates were analysed by Western blot

972   using 1D8 anti-MT1-MMP and anti-actin antibodies. Arrows point bands of interest.

973   Quantification of the cell surface MT1-MMP in the left panel is shown as a graph (right

974   panel). MT1-MMP band intensities were normalized by actin band. Data are presented as

975   mean ± SD. (n=5)

976   **b.** HT1080 cells transfected with siRNAs targeting KIFs were subjected to indirect

977   immunofluorescent staining with anti-MT1-MMP antibody without permeabilization and

978   imaged with confocal microscopy. Representative extended focus images of three

979   independent experiments were shown for MT1-MMP (red) and actin (yellow) (top panel).

980   Quantitative data were shown as a graph (bottom panel). Fluorescent intensity of extended

981   focus image per cell was measured and the data are presented as mean ± SD.

982   **c.** HT-1080 cells transfected with siRNAs targeting the KIFs were stained with anti-MT1-

983   MMP antibody without permeabilization (red) and imaged by TIRF microscopy.

984   Representative images of three independent experiments are shown (left panel). Scale bars

985   are 10 µm. Quantitative data of the fluorescent intensities at the substrate-attachment side

986   were shown as a graph (right panel). Data are presented as mean ± SD. (n=30). ****$P <$

987   0.0001; **$P <$ 0.01; n.s., non-significant.

988   **d.** HT-1080 cells were transfected with siRNAs targeting the selected KIFs. After 72 hours,

989   cells were stained with anti-β1 integrin (green) antibody without permeabilisation and imaged

990   by TIRF microscopy. Representative images of three independent experiments are shown

991   (top panel). Scale bars are 10 µm. Quantification of β1 integrin expression at the substrate

992   attachment side in HT-1080 cells were shown as a graph (bottom panel). Data are

993   presented as mean ± SD. (n=30).

994

995 **Figure 3. The knockdown of KIF13A, KIF3A, KIF9 and KIF1C diminishes MT1-MMP-**

996 **dependent cell migration in 3D collagen.**

997 **a.** HT1080 cells transfected with siRNA indicated were subjected to the same invasion assay

998 and data shown as a graph (bottom right panel). Data are presented as mean of the number

999 of cells migrated through six trans-wells for each treatment and are representative of three

1000 independent experiments. **** $P < 0.0001$, ** $P < 0.001$, n.s., non-significant.

1001 **b.** HT1080 cells were transfected with siRNAs targeting the selected KIFs and subjected to

1002 bead invasion assay in the presence or absence of GM6001 (10 µM). A representative

1003 image of cells migrating from the surface of the bead into collagen type-I matrix (2mg/ml) is

1004 shown (top panel). Scale bar,130 µm. Data are presented as mean of the distance migrated

1005 by one hundred cells for each treatment. Error bars SD, **** $P < 0.0001$, n.s., non-

1006 significant.

1007 **c.** HT1080 cells were transfected with siRNAs targeting the selected KIFs and subjected to

1008 wound healing assay on plastic. Images of 0h and 6h time points are shown. Images are

1009 representative of three independent experiments. Red lines highlight the migration front.

1010 Scale bar, 200 µm. Quantification of wound healing assay data were shown as a graph

1011 (bottom panel). Data are presented as mean of the percentage of wound closure relative to

1012 the initial gap area. * $P < 0.019$.

1013

1014 **Figure 4. MT1-RFP and KIF-GFP co-localisation in HT-1080 cells cultured on gelatin-**

1015 **coated cover glass and within 3D collagen matrix.**

1016 **a, b, c, d, e.** HT-1080 cells transfected with GFP-tagged KIFs (indicated, green) and MT1-

1017 RFP (red) were cultured on gelatin-coated cover glass. Extended focus representative

1018 images are shown. White boxes enclose enlarged areas for perinuclear region and orange

1019 boxes for periphery region. Scale bars indicate 10 µm.

1020 **f.** Quantification of co-localisation between GFP-tagged KIFs and MT1-RFP. Data are

1021 presented as the mean of 20 PCC calculated for 20 different cells per treatment and are

1022 representative of three independent experiments. One-way ordinary Anova with Tuckey's

1023 multiple comparisons test. Data are shown as mean ± SD. **** $P < 0.0001$: * $P < 0.05$; ** $P <$

1024 0.01; n.s., non-significant.

1025 **g, h, i, j, k.** HT-1080 cells transfected with GFP-tagged KIFs (green) and MT1-RFP (red)

1026 were cultured within 3D collagen gel and imaged by confocal microscopy. Extended focus

1027 representative images and the corresponding orthogonal views are shown. White boxes

1028 enclose enlarged areas. Scale bars are 25 µm.

1029 **l.** Quantification of co-localisation between GFP-tagged KIFs and MT1-RFP. Data are

1030 presented as the mean of five PCCs calculated for five different cells per treatment and are

1031 representative of three independent experiments. One-way ordinary Anova with Tuckey's

34

1032 multiple comparisons test. Data are presented as mean ± SD; ***P* < 0.01; ****P* < 0.001; *****P*

1033 < 0.0001; n.s., non-significant.

1034

1035

1036 **Figure 5. MT1-RFP was co-trafficked with KIF13A-GFP and KIF3A-GFP**

1037 **a, b.** HT-1080 cells were transfected with KIF13A-GFP (green) and MT1-RFP (red) and they

1038 were subjected to live cell imaging by confocal microscopy. Representative image time

1039 sequences are shown. White arrows point vesicles of interest. Scale bars are 22 μm.

1040 **c.** Quantification of mean velocity of vesicles of interest at the leading edge and nuclear

1041 area. Data are representative of five independent experiments and are calculated for 47 and

1042 44 trajectories for the cell edge and the peri-nuclear area respectively. Unpaired T test with

1043 Welch's correction. Data are shown as mean ± SD. n.s., non-significant.

1044 **d.** Quantification of vesicle diameter at the cell edge and peri-nuclear area. Data are

1045 representative of five independent experiments and are calculated for 129 vesicles for the

1046 leading edge and the peri-nuclear area. Data are shown as mean ± SD. *** P < 0.001.

1047 **e, f.** HT-1080 cells transfected with KIF13A-GFP (green) and MT1-RFP (red) were subjected

1048 to live cell imaging by TIRF microscopy. Representative image time sequences are shown.

1049 White arrows point vesicles of interest. IRM, internal reflection microscopy. Scale bar is 10

1050 μm.

1051 **g, h.** HT-1080 cells transfected with KIF3A-GFP (green) and MT1-RFP (red) and they were

1052 subjected to live cell imaging by confocal microscopy. Representative image time sequences

1053 are shown. White arrows point vesicles of interest. Scale bars are 22 μm.

1054 **i.** Quantification of mean velocity of vesicles of interest with linear or oscillatory trajectories.

1055 Data are representative of five independent experiments and are calculated for 26 and 24

1056 linear and oscillatory trajectories respectively. Unpaired T test with Welch's correction. Data

1057 are shown as mean ± SD. n.s., non-significant.

1058 **j**. Quantification of vesicle diameter. Data are representative of five independent

1059 experiments and are calculated for 129 vesicles for each group. Unpaired T test with

1060 Welch's correction was used. Data are shown as mean ± SD. n.s., non-significant.

1061

1062 **Figure 6. Time lapse imaging of cells expressing MT1-RFP, KIF9-v1-GFP, KIF9-v2-**

1063 **GFP, and KIF1C-GFP.**

1064 **a.** HT-1080 cells transfected with KIF9-v1-GFP (green) and MT1-RFP (red) were subjected

1065 to live cell imaging by confocal microscopy. Representative image sequence is shown.

1066 White arrows point vesicles of interest. Scale bar is 22 μm.

1067   **b.** HT-1080 cells were transfected with KIF9-v2-GFP (green) and MT1-RFP (red) and they
1068   were subjected to live cell imaging by confocal microscopy. Representative image time
1069   sequence is shown. Scale bars are 22 µm.

1070   **c.** HT-1080 cells were transfected with KIF1C-GFP (green) and MT1-RFP (red) and they
1071   were subjected to live cell imaging by confocal microscopy. Representative image time
1072   sequences are shown. White arrows point trailing edges. Scale bars are 22 µm.

1073

1074   **Figure 7. KIF13A and KIF3A transport MT1-MMP-containing vesicles.**

1075   **a.** HT-1080 cells were transfected with siRNAs targeting the selected KIFs and subjected to
1076   gelatin film degradation assay in the presence or absence of GM6001 (10 µM). Scale bars
1077   are130 µm.

1078   **b**. Quantification of the degradation area (μm^2) per cell in HT1080 cells transfected with the
1079   specified siRNAs. Data are presented as mean of 10 independent microscopic fields of view
1080   and are representative of three independent experiments. One-way ordinary Anova with
1081   Tuckey's multiple comparisons test. Data are shown as mean ± SD. ****$P < 0.0001$; ***$P <$
1082 0.001; **$P < 0.01$; n.s., non-significant.

1083   **c**. Efficiency of KIF knockdown was assessed by one-step RT-PCR. Quantification of
1084   KIF13A and KIF3A mRNA fold changes relative to GADPH mRNA. The data are
1085   representative of three independent experiments.

1086   **d, e, f.** HT-1080 cells were transfected with KIF13A-GFP (green), KIF3A-GFP (white) and
1087   MT1-RFP (red) and they were subjected to live cell imaging by confocal microscopy.
1088   Representative image time sequences are shown. Arrows point vesicles of interest. Scale
1089   bars are 22 µm.

1090   **g.** Quantification of mean velocities of MT1-RFP-containing vesicles transported by KIF13A-
1091   GFP at the cell edge and nuclear area. Data are representative of three independent
1092   experiments and are calculated for 32 and seven trajectories for the cell edge and the
1093   nuclear area respectively. Unpaired T test with Welch's correction. Data are shown as mean
1094   ± SD. **$P < 0.01$; n.s., non-significant.

1095   **h.** Quantification of mean velocities of MT1-RFP-containing vesicles transported by KIF3A-
1096   GFP with linear or oscillatory trajectories. Data are representative of three independent
1097   experiments and are calculated for 10 linear and 11 oscillatory trajectories. Unpaired T test
1098   with Welch's correction. Data are shown as mean ± SD. **$P < 0.01$, n.s., non-significant.

1099

1100

1101   **Figure 8. Increased gelatin film degradation upon KIF9 knockdown is due to increased**
1102   **KIF13A and KIF3A-dependent vesicle transport of MT1-MMP**

1103   **a**. HT1080 cells were transfected with siRNA for KIF13A, KIF3A and/or KIF9 and subjected

1104   to gelatin film degradation assay. Cells wer counterstained with DAPI (lower panels). Scale

1105   bar is 130µm.

1106   **b**. Quantification of the degradation area (µm^2) per cell. Data are presented as the mean of

1107   ten independent microscopic fields of view and are representative of three independent

1108   experiments. *P* values were calculated by Student T test. Data are shown as mean ± S.D.

1109   *****p*>0.0001; **p*>0.05.

1110   **c**. Efficiency of KIF knockdown by one-step RT-PCR. Quantification of KIF13A, KIF3A and

1111   KIF9-v1 mRNA fold changes relative to GADPH. The data are representative of three

1112   independent experiments.

1113

1114   **Figure 9. Effect of KIF knockdown on MT1-MMP activity in RASF and MDA-MB-231**

1115   **cells.**

1116   **a.** RASFs were transfected with siRNAs targeting the selected KIFs and subjected to

1117   collagen film degradation assay in the presence or absence of GM6001 (10 µM). Scale bars,

1118   130 µm.

1119   **b.** Quantitative data of the integrated density of the collagen layer in RASFs transfected with

1120   the specified siRNAs. Data are presented as mean of eight independent microscopic fields

1121   of view and are representative of five independent experiments. One-way ordinary Anova

1122   with Tuckey's multiple comparisons test. Data are shown as mean ± SD. *****P* < 0.0001, ***P*

1123   < 0.01, **P* < 0.05, n.s., non-significant.

1124   **c.** Efficiency of KIF knockdown assessed by RT-PCR in RASFs were shown as graphs. The

1125   data are representative of three independent experiments.

1126   **d.** MDA-MB-231 cells were transfected with siRNAs targeting the indicated KIFs and

1127   subjected to gelatin film degradation assay in the presence or absence of GM6001 (10 µM).

1128   Scale bars are 130 µm. **e.** Quantitative data of the degradation area (µm^2) per cell were

1129   shown as a graph. Data are presented as the mean of fifteen independent microscopic fields

1130   of view and are representative of five independent experiments. *P* values were calculated by

1131   One-way ordinary Anova with Tuckey's multiple comparisons test. Data are shown as mean

1132   ± SD; *****P* < 0.0001. n.s., non-significant.

1133   **f.** Efficiency of knockdown for KIF13A and KIF9 were assessed by RT-PCR. The level of

1134   mRNAs relative to GADPH mRNA were shown as graphs. Efficiency of KIF3A and KIF1C

1135   knockdown were assessed by Western blot. Cell lysates were analysed by Western blotting.

1136   Quantification of the intensity of KIF3A, KIF1C and KIF5B protein bands relative to actin

1137   were shown as graphs. The data are representative of three independent experiments.

1138

1139 **Figure 10. Genomic analysis of KIF13A and KIF9.**

1140 **a.** The oncoprints of KIF13A and KIF9 were identified. Genetic alterations of KIF13A and

1141 KIF9. The columns represent patients from studies within TCGA and the rows gene

1142 alterations like amplification and deep deletion.

1143 **b.** Genetic alterations of KIF13A summarised according to the study type. Amplifications are
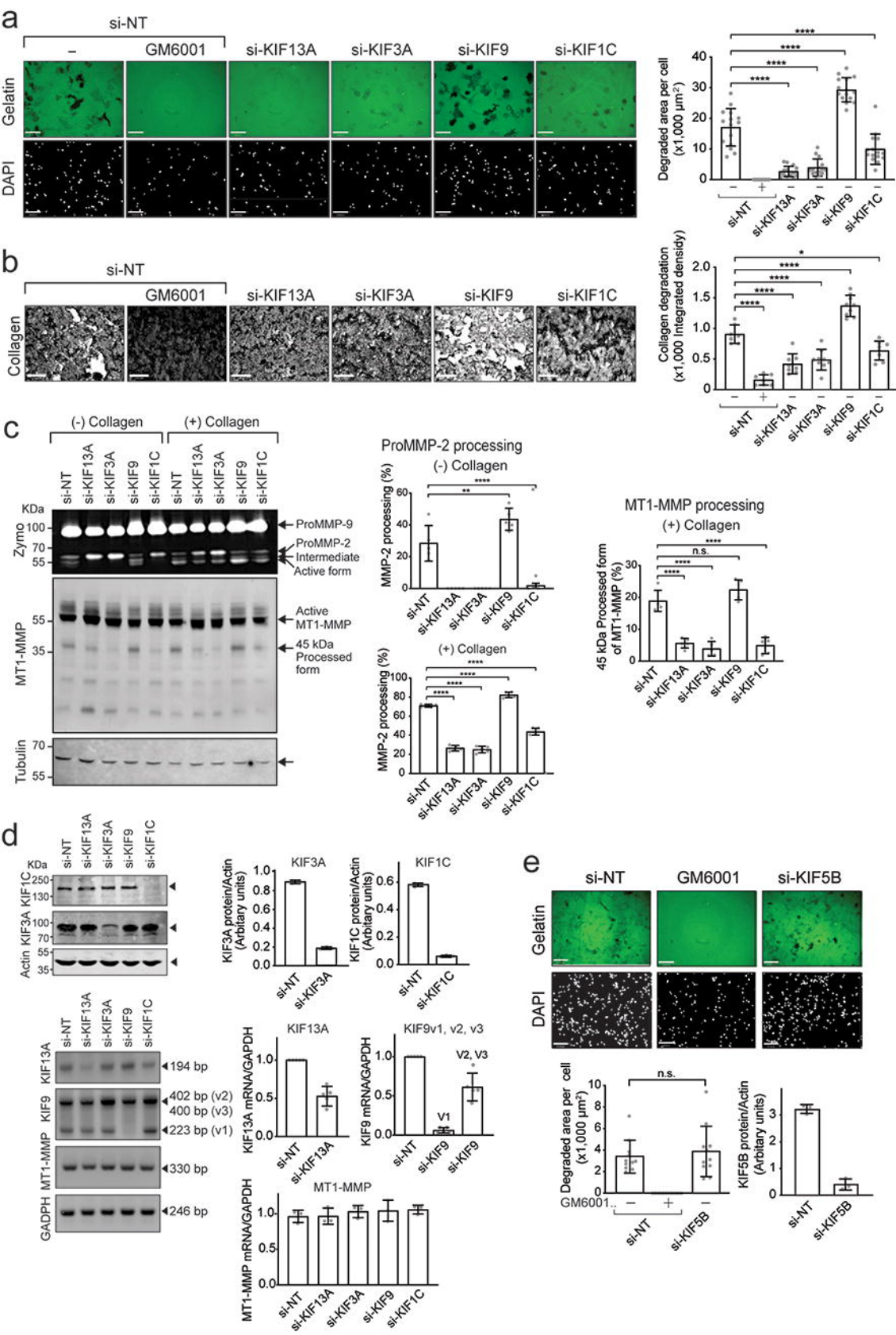
1144 shown in red and deep deletions are blue.

1145 **c.** Genetic alterations of KIF9 summarised according to the study type. Amplifications are

1146 shown in red and deep deletions are blue.

1147 **d.** Kaplan-Meier survival analysis of liver cancer patients with low or high mRNA expression

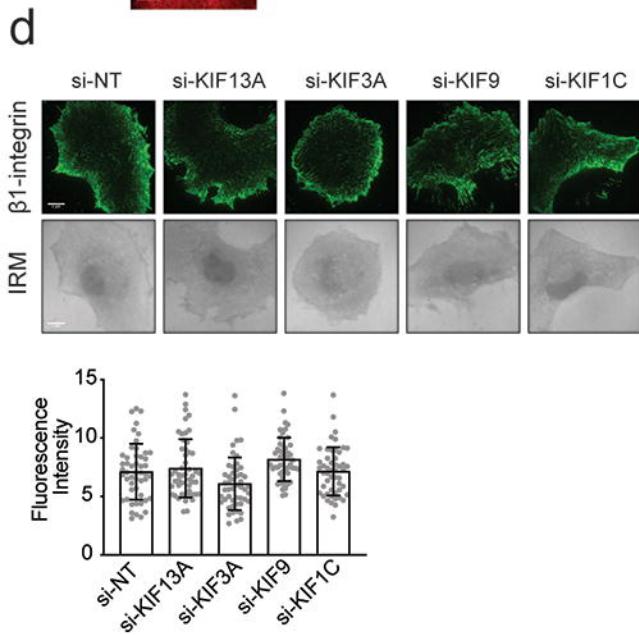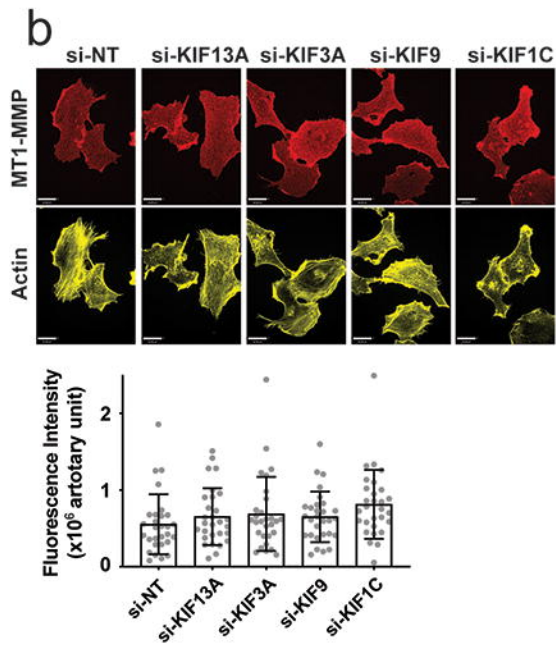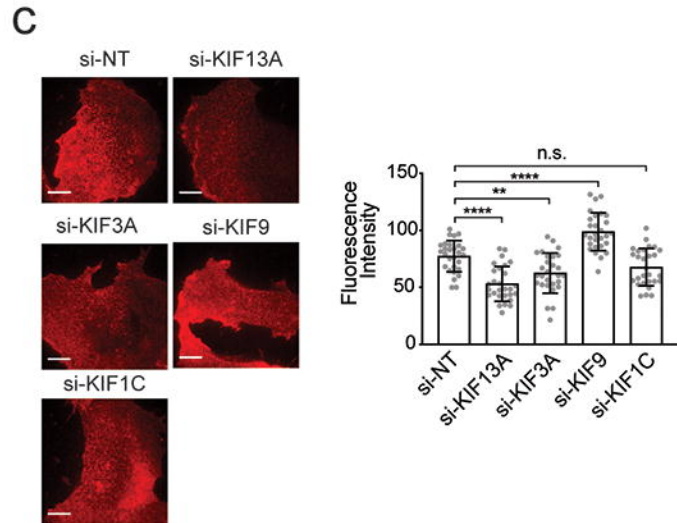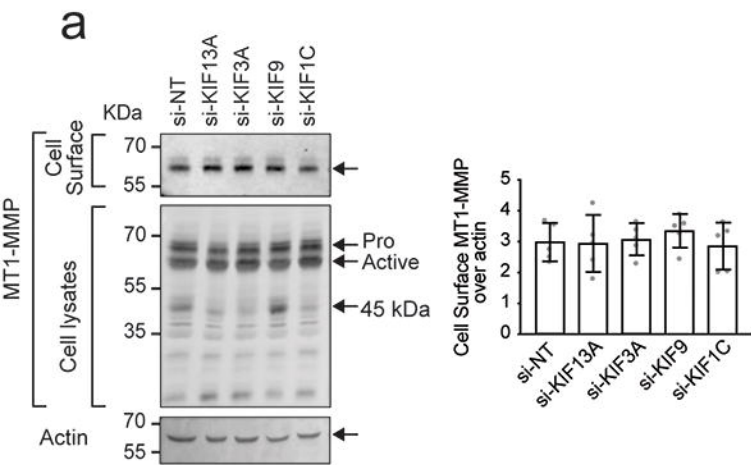1148 of KIF13A. P value was obtained with log-rank test.

1149 **e.** Kaplan-Meier survival analysis of renal cancer patients with low or high mRNA expression

1150 of KIF9. *P* value was obtained with log-rank test. **f.** Kaplan-Meier survival analysis of

1151 colorectal cancer patients with low or high mRNA expression of KIF9. *P* value was obtained
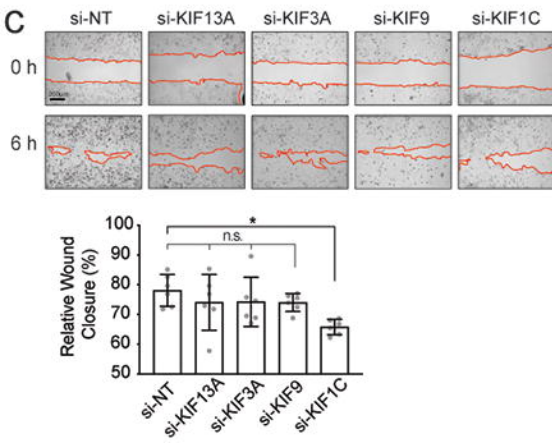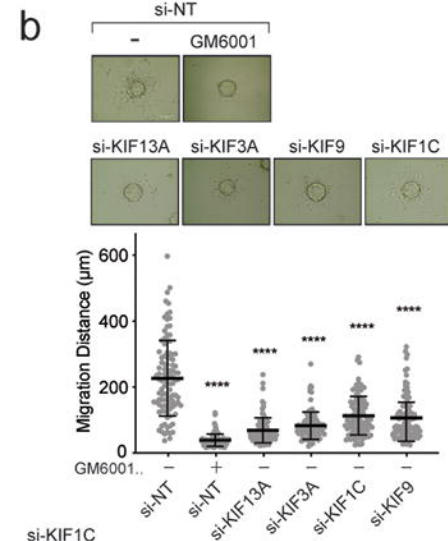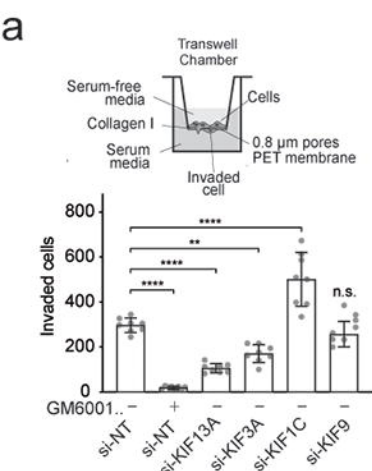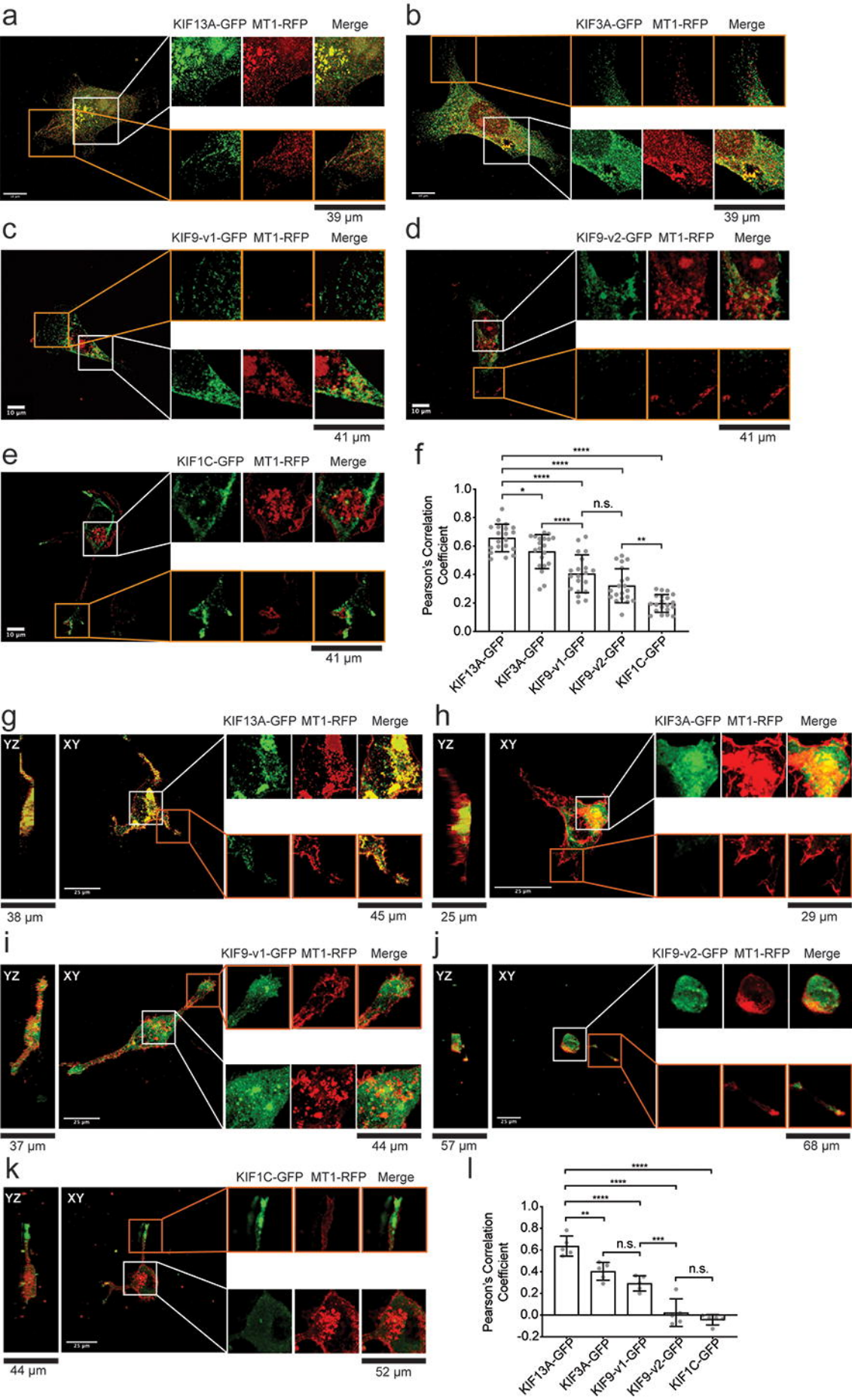
1152 with log-rank test.

1153

1154
1155

a

MT1-MMP

Cell Surface

KDa | si-NT | si-KIF13A | si-KIF3A | si-KIF9 | si-KIF1C

70 — 55 — ← (arrow)

Cell lysates

70 — ← Pro
← Active
55 —
← 45 kDa
35 —

Actin

70 — 55 — ← (arrow)

Cell Surface MT1-MMP over actin (bar graph, y-axis 0–5): si-NT, si-KIF13A, si-KIF3A, si-KIF9, si-KIF1C

b

si-NT | si-KIF13A | si-KIF3A | si-KIF9 | si-KIF1C

MT1-MMP

Actin

Fluorescence Intensity (×10^6 arbitrary unit) (bar graph, y-axis 0–2): si-NT, si-KIF13A, si-KIF3A, si-KIF9, si-KIF1C

c

si-NT | si-KIF13A
si-KIF3A | si-KIF9
si-KIF1C

Fluorescence Intensity (bar graph, y-axis 0–150): n.s., ****, **, ****
si-NT, si-KIF13A, si-KIF3A, si-KIF9, si-KIF1C

d

si-NT | si-KIF13A | si-KIF3A | si-KIF9 | si-KIF1C

β1-integrin

IRM

Fluorescence Intensity (bar graph, y-axis 0–15): si-NT, si-KIF13A, si-KIF3A, si-KIF9, si-KIF1C

a

Transwell Chamber

Serum-free media — Cells
Collagen I — 0.8 μm pores PET membrane
Serum media — Invaded cell

Invaded cells (y-axis: 0 to 800)

GM6001.. — + — — — —

si-NT, si-NT, si-KIF13A, si-KIF3A, si-KIF1C, si-KIF9

**** **** ** n.s.

b

si-NT
– GM6001

si-KIF13A si-KIF3A si-KIF9 si-KIF1C

Migration Distance (μm) (y-axis: 0 to 600)

GM6001.. — + — — — —

si-NT, si-NT, si-KIF13A, si-KIF3A, si-KIF1C, si-KIF9

**** **** **** **** ****

c

si-NT si-KIF13A si-KIF3A si-KIF9 si-KIF1C

0 h

6 h

Relative Wound Closure (%) (y-axis: 50 to 100)

si-NT, si-KIF13A, si-KIF3A, si-KIF9, si-KIF1C

n.s. *

a

0 s 3 s 6 s 9 s 12 s

KIF13A-GFP

MT1-RFP KIF13A-GFP

KIF13A-GFP
MT1-RFP

Merge

12 µm

b

0 s 20 s 40 s

KIF13A-GFP

MT1-RFP KIF13A-GFP

KIF13A-GFP
MT1-RFP

Merge

12 µm

c

Mean Speed (µm/sec)

n.s.

Cell Periphery Peri-Nuclear Area

d

Vesicle Diameter (µm)

***

Cell Periphery Peri-Nuclear Area

e

KIF13A-GFP
MT1-RFP

10 µm

0 s 3 s

6 s 9 s

KIF13A-GFP
MT1-RFP

10 µm

f

KIF13A-GFP
MT1-RFP

10 µm

0 s 3 s 6 s 9 s 12 s

KIF13A-GFP
MT1-RFP

IRM

10 µm

g

0 s 20 s 40 s 60 s 80 s

KIF3A-GFP

MT1-RFP

KIF3A-GFP
MT1-RFP

Merge

KIF3A-GFP
MT1-RFP

12 µm

h

0 s 9 s 18 s

KIF3A-GFP

MT1-RFP

KIF3A-GFP
MT1-RFP

Merge

20 µm

i

Mean Speed (µm/sec)

n.s.

Linear trajectory Oscillatory trajectory

j

Vesicle Diameter (µm)

n.s.

Linear trajectory Oscillatory trajectory

a

KIF9-v1-GFP MT1-RFP

| 0 s | 3 s | 6 s | 9 s | 12 s |

Merge   MT1-RFP   KIF9-v1-GFP

KIF9-v1-GFP
MT1-RFP

12 µm

b

KIF9-v2-GFP MT1-RFP

| 0 s | 30 s | 60 s |

Merge   MT1-RFP   KIF9-v2-GFP

KIF9-v2-GFP
MT1-RFP

20 µm

c

| 0 s | 180 s | 360 s | | 0 s | 180 s | 360 s |

KIF1C-GFP

MT1-RFP

Merge

a

| | si-NT | | GM6001 | si-KIF13A | si-KIF3A | si-KIF13A +si-KIF3A |

b Degraded area per cell (×1,000 μm²)

c KIF13A mRNA (%), KIF3A mRNA (%)

d KIF13A-GFP/ KIF3A-Halo/ MT1-RFP — 0 s, 5 s, 10 s, 15 s, 20 s — KIF13A-GFP, KIF3A-Halo, MT1-RFP, Merge — 20 μm

e KIF13A-GFP, KIF3A-Halo, MT1-RFP — 0 s, 5 s, 10 s, 15 s, 20 s — KIF13A-GFP, KIF3A-Halo, MT1-RFP, Merge — 15 μm

f KIF13A-GFP, KIF3A-Halo, MT1-RFP — 0 s, 6 s, 12 s, 16 s, 22 s — KIF13A-GFP/KIF3A-Halo, Merge — 0 s, 2 s, 4 s, 6 s, 8 s — KIF13A-GFP/KIF3A-Halo, Merge — 20 μm

g KIF13A — Mean Velocity (μm/s) — Cell Edge, Peri-nuclear Area — **

h KIF3A — Mean Velocity (μm/s) — Linear trajectory, Oscillatory trajectory — **

a

Gelatin / DAPI panels: si-NT, GM6001, si-KIF13A, si-KIF3A, si-KIF9, si-KIF13A + si-KIF9, si-KIF3A + si-KIF9

b

Degraded area per cell (×1000 μm²)

GM6001	-	+	-	-	-	-	-
si-NT	+	+	-	-	-	-	-
si-KIF13A	-	-	+	-	-	+	-
si-KIF3A	-	-	-	+	-	-	+
si-KIF9	-	-	-	-	+	+	+

**** **** **** **** * ****

c

KIF13A mRNA normalised to GADPH (%): si-NT, si-KIF13, si-KIF9, si-KIF13A + si-KIF9

KIF3A mRNA normalised to GADPH (%): si-NT, si-KIF3A, si-KIF9, si-KIF3A + si-KIF9

KIF9-v1 mRNA normalised to GADPH (%): si-NT, si-KIF13, si-KIF3, si-KIF9, si-KIF13A + si-KIF9, si-KIF3A + si-KIF9

a

si-NT

GM6001 si-KIF13A

si-KIF3A si-KIF9 si-KIF1C

b

Remaining collagen (Integrated density)

n.s.

**

*

****

****

si-NT GM6001 si-KIF13A si-KIF3A si-KIF9 si-KIF1C

c

KIF13A

KIF13A mRNA/GAPDH

si-NT si-KIF13A

KIF3A

KIF3A mRNA/GAPDH

si-NT si-KIF3A

KIF9

KIF9 mRNA/GAPDH

V1 V2, V3

si-NT si-KIF9 si-KIF9

KIF1C

KIF1C mRNA/GAPDH

si-NT si-KIF1C

d

si-NT

GM6001 si-KIF13A si-KIF3A si-KIF9 si-KIF1C si-KIF5B

Gelatin

DAPI

e

Degraded area per cell (×1000 μm²)

n.s.

****

si-NT GM6001 si-KIF13A si-KIF3A si-KIF9 si-KIF1C si-KIF5B

f

KIF13A

KIF13A mRNA/GAPDH

si-NT si-KIF13A

KIF3A

KIF3A Protein/Actin

si-NT si-KIF3A

KIF9

KIF9 mRNA/GAPDH

V1 V2, V3

si-NT si-KIF9 si-KIF9

KIF1C

KIF1C protein/Actin

si-NT si-KIF1C

KIF5B

KIF5B protein/Actin

si-NT si-KIF5B

a

Study of origin		
KIF13A: AMP	1.3%	Amplification
KIF13A: HOMDEL	0.2%	Deep deletion
KIF9: AMP	0.1%	No alterations
KIF9: HOMDEL	0.5%	

b — KIF13A

c — KIF9

Amplification
Deep deletion

Mutation data
CNA data

d — Liver Carcer

p < 0.001

Survival Probability
Years

KIF13A low expression (n=204)
KIF13A high expression (n=161)

e — Renal Carcer

p < 0.001

Survival Probability
Years

KIF9 low expression (n=647)
KIF9 high expression (n=230)

f — Colorectal Carcer

p < 0.001

Survival Probability
Years

KIF9 low expression (n=209)
KIF9 high expression (n=388)